A syndromic neurodevelopmental disorder caused by rare variants in *PPFIA3*

Authors

Maimuna S. Paul, Sydney L. Michener, Hongling Pan, ..., Carlos A. Bacino, Brendan H. Lee, Hsiao-Tuan Chao

Correspondence

chao-lab@bcm.edu

PPFIA3 is a scaffolding protein that mediates synaptic transmission. This study identified 20 individuals with *PPFIA3* variants associated with developmental delay, intellectual disability, hypotonia, dysmorphisms, micro/macrocephaly, autistic features, and epilepsy. Functional analysis shows that *PPFIA3* variants cause a syndromic neurodevelopmental disorder through a potential loss-of-function mechanism.

Paul et al., 2024, The American Journal of Human Genetics *111*, 96–118
January 4, 2024
https://doi.org/10.1016/j.ajhg.2023.12.004

CellPress

ARTICLE

A syndromic neurodevelopmental disorder caused by rare variants in *PPFIA3*

Maimuna S. Paul,[1,2,3] Sydney L. Michener,[1,2,3] Hongling Pan,[2,4] Hiuling Chan,[3,5,6] Jessica M. Pfliger,[1,2,7] Jill A. Rosenfeld,[4] Vanesa C. Lerma,[1,2,8] Alyssa Tran,[4] Megan A. Longley,[1,2] Richard A. Lewis,[4,9] Monika Weisz-Hubshman,[4] Mir Reza Bekheirnia,[4,10] Nasim Bekheirnia,[10] Lauren Massingham,[11] Michael Zech,[12,13,14] Matias Wagner,[12,13,15] Hartmut Engels,[16] Kirsten Cremer,[15] Elisabeth Mangold,[15] Sophia Peters,[15] Jessica Trautmann,[15] Jessica L. Mester,[17] Maria J. Guillen Sacoto,[17]

(Author list continued on next page)

Summary

PPFIA3 encodes the protein-tyrosine phosphatase, receptor-type, F-polypeptide-interacting-protein-alpha-3 (PPFIA3), which is a member of the LAR-protein-tyrosine phosphatase-interacting-protein (liprin) family involved in synapse formation and function, synaptic vesicle transport, and presynaptic active zone assembly. The protein structure and function are evolutionarily well conserved, but human diseases related to PPFIA3 dysfunction are not yet reported in OMIM. Here, we report 20 individuals with rare *PPFIA3* variants (19 heterozygous and 1 compound heterozygous) presenting with developmental delay, intellectual disability, hypotonia, dysmorphisms, microcephaly or macrocephaly, autistic features, and epilepsy with reduced penetrance. Seventeen unique *PPFIA3* variants were detected in 18 families. To determine the pathogenicity of *PPFIA3* variants *in vivo*, we generated transgenic fruit flies producing either human wild-type (WT) PPFIA3 or five missense variants using GAL4-UAS targeted gene expression systems. In the fly overexpression assays, we found that the *PPFIA3* variants in the region encoding the N-terminal coiled-coil domain exhibited stronger phenotypes compared to those affecting the C-terminal region. In the loss-of-function fly assay, we show that the homozygous loss of fly *Liprin-α* leads to embryonic lethality. This lethality is partially rescued by the expression of human PPFIA3 WT, suggesting human PPFIA3 function is partially conserved in the fly. However, two of the tested variants failed to rescue the lethality at the larval stage and one variant failed to rescue lethality at the adult stage. Altogether, the human and fruit fly data reveal that the rare *PPFIA3* variants are dominant-negative loss-of-function alleles that perturb multiple developmental processes and synapse formation.

Introduction

Synapses are highly specialized communication junctions between neurons and their target cells where neurotransmitter release occurs in an intricately coordinated manner. In the presynaptic neuron, a key site for neurotransmitter release is the active zone, which is composed of a complex protein matrix.[1–4] RIM, ELKS, Munc13, RIM-BP, Piccolo/Bassoon, and Liprin-α are the six major protein families comprising the active zone.[5] These active zone proteins, along with other cytoskeletal proteins, Ca^{2+} channels, and soluble N-ethylmaleimide-sensitive fusion attachment protein receptors (SNAREs), form a tightly orchestrated unit to mediate synaptic vesicle docking, priming, fusion, and neurotransmitter release.[5] Prior studies revealed that disruption of synapse structure or function leading to variable defects in neurotransmitter release contributes to neurodevelopmental and neuropsychiatric disorders including epilepsy, intellectual disability (ID), autism spectrum disorder (ASD), schizophrenia, and bipolar disorder.[6–10]

The network of multidomain proteins comprising the active zone falls into different categories such as cytoskeletal and scaffolding proteins, adhesion molecules, calcium channels, and synaptic vesicle release machinery. Liprins are scaffolding proteins found in the presynaptic active zone that are also known as protein tyrosine phosphatase receptor type F polypeptide (PTPRF)-interacting protein α (PPFIA) or β (PPFIB). Liprin family members interact with the adhesion molecule leukocyte antigen receptor-protein

[1]Department of Pediatrics, Section of Neurology and Developmental Neuroscience, Baylor College of Medicine, Houston, TX, USA; [2]Jan and Dan Duncan Neurological Research Institute, Texas Children's Hospital, Houston, TX, USA; [3]Cain Pediatric Neurology Research Foundation Laboratories, Jan and Dan Duncan Neurological Research Institute, Houston, TX, USA; [4]Department of Molecular and Human Genetics, Baylor College of Medicine, Houston, TX, USA; [5]Augustana College, Rock Island, IL, USA; [6]Summer Undergraduate Research Training (SMART) Program, Baylor College of Medicine, Houston, TX, USA; [7]Graduate Program in Electrical and Computer Engineering, Rice University, Houston, TX, USA; [8]Department of Psychology, University of Houston, Houston, TX, USA; [9]Department of Ophthalmology, Baylor College of Medicine, Houston, TX, USA; [10]Renal Genetics Clinic, Baylor College of Medicine, Houston, TX, USA; [11]Rhode Island Hospital and Hasbro Children's Hospital, Providence, RI, USA; [12]Institute of Neurogenomics, Helmholtz Zentrum München, Munich, Germany; [13]Institute of Human Genetics, School of Medicine, Technical University, Munich, Germany; [14]Institute for Advanced Study, Technical University of Munich, Garching, Germany; [15]Division of Pediatric Neurology, Developmental Neurology and Social Pediatrics, Dr. von Hauner Children's Hospital, Munich, Germany; [16]Institute of Human Genetics, School of Medicine, University Hospital Bonn, University of Bonn, Bonn, Germany; [17]GeneDx, Gaithersburg, MD, USA; [18]Epilepsy NeuroGenetics Initiative (ENGIN), Division of Neurology, Children's Hospital of Philadelphia,

(Affiliations continued on next page)

Richard Person,[17] Pamela P. McDonnell,[18,19] Stacey R. Cohen,[18] Laina Lusk,[18] Ana S.A. Cohen,[20] Jean-Baptiste Le Pichon,[21] Tomi Pastinen,[20,22] Dihong Zhou,[23] Kendra Engleman,[23] Caroline Racine,[24,25,26] Laurence Faivre,[26,27] Sébastien Moutton,[26,27] Anne-Sophie Denommé-Pichon,[24,25,26] Hyun Yong Koh,[1,28] Annapurna Poduri,[28] Jeffrey Bolton,[28] Cordula Knopp,[29] Dong Sun Julia Suh,[29] Andrea Maier,[30] Mehran Beiraghi Toosi,[31,32] Ehsan Ghayoor Karimiani,[33,34] Reza Maroofian,[35] Gerald Bradley Schaefer,[36] Vijayalakshmi Ramakumaran,[37] Pradeep Vasudevan,[37] Chitra Prasad,[38] Matthew Osmond,[39] Sarah Schuhmann,[40] Georgia Vasileiou,[40] Sophie Russ-Hall,[41] Ingrid E. Scheffer,[41,42] Gemma L. Carvill,[43] Heather Mefford,[44] Undiagnosed Diseases Network, Carlos A. Bacino,[4,45] Brendan H. Lee,[4,45] and Hsiao-Tuan Chao[1,2,3,4,45,46,47,*]

tyrosine phosphatases (LAR-PTPs) and are subdivided into liprin-α and liprin-β proteins.[11,12] In conjunction with LAR-PTPs, liprins play a key role in the active zone organization and structure. Structural studies show that liprins, including PPFIA3, are comprised of an N-terminal coiled-coil domain and C-terminal sterile-α-motif (SAM) domain.[11,12] The N-terminal coiled-coil domain mediates homodimerization and heterodimerization with other liprin-α members and interactions with other active zone proteins such as RIM and ELKS.[13–16] The SAM domains are known for mediating protein-protein interactions and binding with RNA.[17] The liprin-α SAM domain interacts with the LAR intracellular domain.[18] Apart from these functional domains, liprins also contain intrinsically disordered regions that lack an ordered three-dimensional structure but were previously shown to be important for protein's function.[19,20] Additionally, liprins interact with kinesin motor proteins[21–23] and are involved in the hedgehog signaling-dependent trafficking of Kif7 and Gli to the cilia in the context of embryonic development and cortical microtubule organization.[21,22]

Vertebrates have four Ppfia (1–4) proteins and two Ppfib (1–2) proteins that are encoded by *Ppfia1–4* or *Ppfib1–2*, respectively.[12] Expression studies in mice show that all four mouse *Ppfia1–4* orthologs are expressed in the brain with differences in distribution and expression levels.[24] Ppfia1 is found in the brain, lung, heart, liver, muscle, spleen, and testes.[12,25,26] In the brain, Ppfia1 is predominantly localized to the cerebellum and olfactory bulb.[24–26] In contrast, Ppfia2, Ppfia3, and Ppfia4 are predominantly found in the brain,[12,25,26] including structures such as the olfactory bulb, striatum, cortex, hippocampus, thalamus, midbrain, cerebellum, and brainstem.[24–26] A subcellular localization study showed that Ppfia2 and Ppfia3 are located in both the pre-synaptic and post-synaptic compartments.[26] However, only Ppfia3 specifically co-localizes in the presynaptic compartment and mediates protein-protein interactions with the active zone proteins Bassoon, RIM, Munc-13, RIM-BP, and ELKS in hippocampal neurons.[27] In humans, transcriptomic studies revealed that *PPFIA3* (MIM: 603144) is similarly expressed in different brain regions like the neocortex, striatum, hippocampus, amygdala, mediodorsal nucleus of the thalamus, and cerebellar cortex from the early embryonic stage to late adulthood.[28]

Ppfia proteins are well conserved in both vertebrates and invertebrates. In *C. elegans*, the sole Ppfia ortholog, *syd-2,* plays a key role in presynaptic active zone organization.[29,30] Studies showed that syd-2 recruits synaptic components to presynaptic sites and contributes to the formation of neuromuscular junctions (NMJs), along with active zone assembly and stabilization.[30,31] Mutant *syd-2* worms show presynaptic active zone defects due to disruption of syd-2 oligomerization.[13,30,31] A similar role was found for the fruit fly ortholog *Liprin-α* where it is required for synapse formation, synaptic vesicular transport, active zone

Philadelphia, PA, USA; [19]Department of Neurology, Perelman School of Medicine, University of Pennsylvania, Philadelphia, PA, USA; [20]Children's Mercy Kansas City, Genomic Medicine Center, The University of Missouri-Kansas City (UMKC), School of Medicine, Kansas City, MO, USA; [21]Department of Pediatrics, Children's Mercy Kansas City, Kansas City, MO, USA; [22]Children's Mercy Research Institute, Kansas City, MO, USA; [23]Children's Mercy Hospital, Kansas City, MO, USA; [24]University Hospital, Dijon, France; [25]INSERM UMR1231 GAD "Génétique des Anomalies Du Développement," FHU-TRANSLAD, University of Burgundy, Dijon, France; [26]Functional Unit for Diagnostic Innovation in Rare Diseases, FHU-TRANSLAD, Dijon Bourgogne, France; [27]Department of Genetics and Reference Center for Development Disorders and Intellectual Disabilities, FHU-TRANSLAD and GIMI Institute, Dijon Bourgogne University Hospital, Dijon, France; [28]Department of Neurology, Boston Children's Hospital, Boston, MA, USA; [29]Institute for Human Genetics and Genomic Medicine, Medical Faculty, RWTH, Aachen University, Aachen, Germany; [30]Medical Treatment Center for Adults with Intellectual Disabilities and/or Severe Multiple Disabilities (MZEB), RWTH Aachen University Hospital, Aachen, Germany; [31]Department of Pediatrics, School of Medicine, Mashhad University of Medical Sciences, Mashhad, Iran; [32]Neuroscience Research Center, Mashhad University of Medical Sciences, Mashhad, Iran; [33]Department of Medical Genetics, Next Generation Genetic Polyclinic, Mashhad, Iran; [34]Molecular and Clinical Sciences Institute, St. George's, University of London, Cranmer Terrace, London, UK; [35]Department of Neuromuscular Diseases, UCL Queen Square Institute of Neurology, London, UK; [36]University of Arkansas for Medical Sciences; Little Rock, AR, USA; [37]LNR Genomics Medicine, University Hospitals of Leicester, Leicester, UK; [38]London Health Sciences Centre, and Division of Medical Genetics, Department of Pediatrics, Western University, London, ON, Canada; [39]Children's Hospital of Eastern Ontario Research Institute, University of Ottawa, ON, Canada; [40]Institute of Human Genetics, Universitätsklinikum Erlangen, Friedrich-Alexander-Universität Erlangen-Nürnberg, Erlangen, Germany; [41]Epilepsy Research Centre, Department of Medicine, University of Melbourne, Austin Health, VIC, Australia; [42]Department of Pediatrics, University of Melbourne, Royal Children's Hospital, Florey and Murdoch Children's Research Institutes, VIC, Melbourne, Australia; [43]Department of Neurology, Northwestern University Feinberg School of Medicine, Chicago, IL, USA; [44]Center for Pediatric Neurological Disease Research, St. Jude Children's Research Hospital, Memphis, TN, USA; [45]Texas Children's Hospital, Houston, TX, USA; [46]Department of Neuroscience, Baylor College of Medicine, Houston, TX, USA; [47]McNair Medical Institute, The Robert and Janice McNair Foundation, Houston, TX, USA
*Correspondence: chao-lab@bcm.edu
https://doi.org/10.1016/j.ajhg.2023.12.004.

assembly, and axonal target selection from the retina to the medulla in the central nervous system.[32–34] Consistent with the invertebrate models, synaptic ultrastructure and electrophysiological studies in *Ppfia3* knockout mice found impaired presynaptic active zone assembly, synaptic vesicle docking, tethering, and exocytosis.[27] Altogether, these studies reveal that Ppfia family members are integral scaffolding proteins for the assembly of intricate protein complexes involved in synapse formation, synaptic transmission, and protein trafficking.

Here, we report a cohort of 20 individuals from 18 families with rare variants in *PPFIA3* associated with developmental delay (DD), ID, dysmorphisms, microcephaly, macrocephaly, hypotonia, ASD or autistic features, abnormal electroencephalogram (EEG), and epilepsy. The phenotypic consequences of rare variants in *PPFIA3* have not been previously reported in Online Mendelian Inheritance in Man (OMIM).[35] In a statistical model of *de novo* variants for ASDs/IDs, *PPFIA3* was identified as one of ~1,000 genes significantly lacking functional variation in non-ASD/ID individuals but enriched with *de novo* variants in individuals with ASD/ID.[36] Furthermore, Genome Aggregation Database (gnomAD) version 2.1.1 analysis showed that *PPFIA3* has a high probability of loss-of-function (LOF) intolerance (LOEUF = 0.12, pLI = 1.0), as 64.1 LOF variants were expected given the gene size and guanine-cytosine (GC) content, but only three LOF variants were observed.[37] *PPFIA3* is also a highly constrained gene with a missense *Z* score of 5.49, suggesting intolerance to missense variation, as 727.5 missense variants were expected but only 311 were observed.[37] Together, these findings support that rare *PPFIA3* variants may cause a neurodevelopmental phenotype.

The pathogenicity of the five *PPFIA3* missense variants were tested using overexpression fly assays, revealing that the *PPFIA3* variants are associated with behavioral, developmental, and NMJ defects. LOF assays with fly *Liprin-α* show that the human *PPFIA3* wild type (WT) partially rescued the *Liprin-α* LOF embryonic lethality whereas three of the five tested variants exhibited impaired rescue of the LOF phenotype. Altogether, we show that rare *PPFIA3* variants are deleterious to protein function with *in vivo* fruit fly assays and lead to a syndromic neurodevelopmental disorder characterized by DD, ID, hypotonia, ASD or autistic features, dysmorphisms, microcephaly or macrocephaly, abnormal EEG, and epilepsy in humans.

Material and methods

Study approval for identification of study participants and clinical phenotyping

Clinical data were acquired after written informed consent was obtained in accordance with the ethical standards of the participating institutional review boards (IRBs) on human research at each respective institution. GeneMatcher was used to form an international collaboration, allowing for comparison of individuals and their variants.[38–40] Collection and analysis of the de-identified clinical cohort was approved by Baylor College of Medicine's IRB. *PPFIA3* heterozygous variants were identified by exome sequencing (ES) through each individual's respective institution. DNA was extracted from peripheral blood mononuclear cells, buccal sample, or fetal skin for ES. ES or Sanger sequencing of the parental samples were performed when feasible to confirm *de novo* or inherited segregation. Paternity was confirmed by the inheritance of rare single-nucleotide polymorphisms from the parents. Sample swap was excluded. Participant identities are not known to anyone outside of the research group. Clinical phenotypes are ascertained by expert review of medical records and the most recent clinical assessment per each individual.

Molecular modeling

Molecular visualization of the PPFIA3 structure was completed with PyMol (the PyMOL Molecular Graphics System, v.2.5.2 Schrödinger, LLC). The crystal structure of PPFIA3 (GenBank: NP_003651.1, Uniprot ID: O75145) was used to build the PPFIA3 structure model in PyMol. Affected residues were altered to the corresponding human variants, and the mutation effects were modeled alongside the native protein. The changes in the PPFIA3 structure were assessed by displaying local polar contacts and residue interactions before and after mutagenesis.

Drosophila melanogaster stocks and maintenance

All the fruit fly stocks used in this study were reared in standard cornmeal- and molasses-based fly food at room temperature (RT, 20°C–21°C) unless otherwise noted. The fruit fly stocks used in the study were either obtained from Bloomington Drosophila Stock Center (BDSC) or generated at the Jan and Dan Duncan Neurological Research Institute. We generated transgenic fly alleles as previously described[41] by utilizing the pUASg-HA-attB vector[42] to express the human *PPFIA3* WT and variant cDNAs with a region encoding a C-terminal hemagglutinin (HA) tag under the control of upstream activating sequence (UAS) elements by Gateway LR Cloning (LR Clonase II, Thermo Fisher Scientific, Cat #11791020). To generate the *PPFIA3* variants, we utilized the human full-length cDNA of *PPFIA3* (GenBank: NM_003660.4). *PPFIA3* c.115C>T (p.Arg39Cys), *PPFIA3* c.943G>T (p.Ala315Ser), *PPFIA3* c.1243C>T (p.Arg415Trp), *PPFIA3* c.1638G>T (p.Trp546Cys), and *PPFIA3* c.2350C>T (p.Arg784Trp) were generated by Q5 site-directed mutagenesis (New England Biolabs, Cat #M0491S) in the pDONR221 Gateway compatible donor vector. The constructs were confirmed by Sanger sequencing. Primer sequences for the site-directed mutagenesis and Sanger sequencing are listed in Table S1. Human *PPFIA3* WT and variant cDNAs were inserted into the chromosome-3 VK33 (PBac{y[+]-attP}VK00033) docking site by φC31-mediated recombination for fruit fly transgenesis.[42] Transgenic UAS fly alleles generated in this study include *UAS-PPFIA3*-WT-HA, *UAS-PPFIA3*-p.Arg39Cys-HA, *UAS-PPFIA3*-p.Ala315Ser-HA, *UAS-PPFIA3*-p.Arg415Trp-HA, *UAS-PPFIA3*-p.Trp546Cys-HA, and *UAS-PPFIA3*-p.Arg784Trp-HA. Fly alleles from the stock centers include *Liprin-α^{F3ex15}/In(2LR)Gla* (BDSC#8563), *w[1118]; Df(2L)Exel7027/CyO* (BDSC#7801), *y[1] w[118]; PBac{y[+]-aatP-3B}-VK00033* (BDSC#9750), and *elav-GAL4/CyO* (BDSC#8765). *UAS*-empty-*VK33*, *Actin-GAL4*, and *da-GAL4* lines were obtained from Dr. Hugo J. Bellen.

Larval brain and NMJ immunostaining and confocal microscopy

Fruit fly larval brains or whole-body wall muscles including the central nervous system were dissected from wandering third-instar larvae reared at 25°C in ice-cold 1X-PBS and fixed in 4% paraformaldehyde for 20 min at RT. The tissues were washed four times in Tri-PBS (1X-PBS +0.2% Triton X-100) with 1% bovine serum albumin (BSA) for 15 min each followed by incubation in blocking solution (Tri-PBS with 0.1% BSA and 8% normal donkey serum) for 30 min. Primary antibodies, rat anti-HA (1:50, clone 3F10, Millipore Sigma, Cat#11867423001), mouse anti-elav (1:100, Developmental Studies Hybridoma Bank, Cat#9F8A9), mouse anti-Bruchpilot (Brp) (1:50, Developmental Studies Hybridoma Bank, Cat#nc82), and goat anti-horseradish peroxidase (HRP) (1:1000, Jackson ImmunoResearch, Cat#123-005-021) were diluted in blocking solution, added to the tissues, and incubated overnight at 4°C. The tissues were rinsed three to four times in Tri-PBS with 1% BSA for 15 min each followed by incubation in blocking solution for 30 min at RT. The secondary antibodies, donkey anti-rat IgG antibody (Cy3) (1:300, Jackson ImmunoResearch, Cat#712-165-153), Alexa Fluor 488 Affinipure donkey anti-goat IgG (H + L) (1:300, Jackson ImmunoResearch, Cat#705-545-147), and Alexa Fluor 488 Affinipure donkey anti-mouse IgG (H + L) (1:300, Jackson ImmunoResearch, Cat#715-545-151) were diluted in blocking solution and added to the tissues for a 90-min incubation at RT on a rocker. For NMJ staining, phalloidin (Phalloidin-iFluor 405 Reagent, Abcam, Cat#ab176752) was added along with the secondary antibodies to visualize the muscles. After removing the secondary antibody, tissues were washed three times in Tri-PBS with 1% BSA for 15 min each and then rinsed in 1X-PBS at RT. For larval brains, this was followed by incubation in 406-diamidino-2-phenylindole dihydrochloride (DAPI, 1 mg/mL, Cayman Chemical, Cat#14285) for 30 min at RT. After removing DAPI, a final wash was completed with 1X-PBS for 15 min at RT. The tissues were mounted in Prolong Glass anti-fade mountant (Thermo Scientific, Cat#36984). Images were acquired on a Leica Sp8 laser-scanning confocal microscope. The same settings for laser power and detector gain were used for all genotypes. Third-instar larval brain images were acquired as a z stack with a z step of 1 μm and line average of four at 400 Hz with a 20× objective at 1024 × 1024 pixel resolution. NMJ images were acquired with a 40× objective. Maximum intensity projections were created from the z stack in ImageJ. All images were processed and assembled using ImageJ and Adobe Illustrator.

Western blotting

Adult fly heads were homogenized using cell lysis buffer (50 mM Tris-HCl, 150 mM NaCl, 0.25% SDS, 0.25% sodium deoxycholate, 1 mM EDTA, and 1X liquid protease inhibitor [Gen DEPOT Cat#P3100-001]). The homogenized fly heads in cell lysis buffer were centrifuged at 13,000 revolutions per minute (rpm) for 10 min at 4°C. The supernatant was collected and mixed with Laemmli buffer containing β-mercaptoethanol and heated at 95°C for 10 min. The samples were loaded in 4%–20% gradient polyacrylamide gels (Bio-Rad MiniPROTEAN TGXTM Cat#4561086) followed by a transfer onto polyvinylidene difluoride membrane (Bio-Rad TransBlot Turbo mini-size LF PVDF membrane). The membrane was blocked using skim milk and treated overnight with the primary antibody (rat anti-HA 1:2000, clone 3F10, Millipore Sigma, Cat#11867423001). Anti-actin hFAB rhodamine antibody (Bio-Rad Cat#12004163, 1:5000) and goat anti-rat IgG polyclonal antibody (IRDye 800CW) (LI-COR Biosciences, Cat#926–32219) were used as the secondary antibodies. Images were acquired on the BioRad Chemidoc Imaging System (Cat#17001401). Quantification was done using ImageJ in which background-subtracted band intensity is acquired for both the actin and HA bands. The average intensity value is normalized and analyzed in GraphPad Prism8. Crosses for the western blot analysis were set up and maintained at 25°C.

Third-instar larval NMJ quantifications

The total number of boutons from abdominal segment 3 (A3) muscle 6/7 were counted semi-manually using Imaris. The spot function was used with point style sphere and radius scale 1.0 to count the number of boutons. The NMJ length was quantified using the HRP staining and measured in ImageJ.

Fruit fly behavioral assays

For the climbing assay, 5-day-old flies of both sexes were anesthetized with CO_2 48 h prior to being tested, and two to three flies were housed in food-containing vials at 25°C. At the time of assay, these flies were transferred without anesthesia to a clear graduated cylinder with a 15-cm mark. The flies were tapped three times to the bottom of the cylinder to examine the climbing ability. The cutoff time to reach the 15-cm mark was 30 s. A total of 55–75 flies of both sexes were tested for each genotype. Crosses for the climbing assay were set up at 25°C and the assay was performed at 20°C–21°C. The climbing assay for 15-day-old flies was done with the flies anesthetized with CO_2 24 h prior to being tested and kept at RT until the behavioral test was done. The cutoff time for the 15-day-old flies to reach the 20-cm mark was 40 s. A total of 40–55 flies of both sexes were tested for each genotype for the 15-day-old flies.

For the bang-sensitivity assay, 5-day-old flies of both sexes were anesthetized with CO_2 48 h prior to being tested, and two to three flies were housed in food-containing vials at 25°C. At the time of assay, these flies were transferred without anesthesia to an empty food vial and vortexed for 10 s. Flies were observed for time to recover from the vortexing. The cutoff time to recover was 30 s. Recovery was defined as being upright and mobile. Flies were considered bang sensitive if they remained upside down, immobile, or showed rhythmic involuntary movements suggestive of electrophysiological abnormalities in the nervous system. A total of 55–75 flies of both sexes were tested for each genotype. Crosses for the bang-sensitivity assay were set up at 25°C, and the assay was performed at 20°C–21°C. The bang-sensitivity assay for 15-day-old flies was done with the flies anesthetized with CO_2 24 h prior to being tested and kept at RT until the behavioral test was done. The vortexing time for the 15-day-old flies was 15 s. A total of 40–55 flies of both sexes were tested for each genotype for the 15-day-old flies.

Liprin-α LOF lethality rescue with human PPFIA3 WT and variants

Df(Liprin-α)/CyO act-GFP; UAS-cDNA/TM6B flies were crossed with *Liprin-α* ^{F3ex15}*/CyO act-GFP; da-GAL4/TM6B* flies. The UAS-cDNA lines used were *UAS*-empty, *UAS-PPFIA3* WT, *UAS-PPFIA3* p.Arg39Cys, *UAS-PPFIA3* p.Arg415Trp, *UAS-PPFIA3* p.Trp546Cys, and *UAS-PPFIA3* p.Arg784Trp. Rescue larvae with the genotype *Df(Liprin-α)/Liprin-α* ^{F3ex15}; *UAS-cDNA/da-GAL4* were selected (GFP negative and Tubby [Tb] negative) and kept in a new vial to assess the development. The experiment was done in three

biological replicates. The crosses were set and maintained at 20°C as the higher temperatures (25°C and above) were embryonic lethal with all cDNAs.

Pupal lethality and eclosion defect assessment

Actin-GAL4/Cyo,Tb females were crossed with the homozygous *UAS-PPFIA3* WT and *UAS-PPFIA3* p.Arg39Cys, p.Ala315Ser, p.Arg415Trp, p.Trp546Cys, and p.Arg784Trp males at 25°C. The overexpression progenies were identified based on the absence of the markers, CyO (visible in adults) and Tb (visible in larvae, pupae, and adults). Sample sizes are shown in Table S2.

Adult fruit fly leg mounting

Adult flies were fixed overnight in ethanol at RT, and the legs were dissected and mounted using CMCP-10 Macroinvertebrate High Viscosity Mountant (D/S259) (Electron Microscopy Sciences, Cat#18004-02). Leg images were taken using the Leica MZ16 stereomicroscope. Images were processed and assembled using Adobe Photoshop CS5.1 and Adobe Illustrator. Crosses were set up at 25°C. Sample sizes are shown in Table S2.

Genomic DNA isolation and qPCR

Genomic DNA was extracted by homogenizing four whole flies in 50 mM sodium hydroxide and heating the samples at 95°C for 30 min followed by the addition of 1 M Tris-HCl (pH 7.5) to stop the lysis. Equal amounts (50 ng) of DNA for each genotype were used for amplification. qPCR was performed with the BioRad SsoAdvanced Universal SYBR-Green Supermix (Cat#1725274) and the BioRad CFX96 Touch Real-Time PCR Detection System (Cat#1845096). The relative change in gene expression was determined by the Livak method, and fold changes were calculated using the $2^{-\Delta\Delta CT}$ formula. The experiment was repeated in three independent biological replicates. *HA* and *PPFIA3* band intensity were quantified by normalizing to the band intensity of the endogenous reference *rps17* and plotted as fold change relative to the control. Flies were maintained at 20°C–21°C. Primer sequences are listed in Table S1.

Statistics

Data was collected and analyzed blinded to genotypes. Statistical analysis between the control and experimental groups was conducted with one-way ANOVA and Tukey's post-hoc analysis in GraphPad Prism 8. Statistical summary is in Table S3.

Results

Identification of rare *PPFIA3* variants in individuals with neurodevelopmental phenotypes

An international collaboration through the Undiagnosed Diseases Network (UDN)[43] and GeneMatcher[38–40] led to the identification of 20 individuals from 18 families with neurodevelopmental phenotypes and 17 rare missense, frameshift deletion, exonic deletion, or consensus splice site variants in *PPFIA3* (Table 1; Figures 1A and 1B, see supplemental information). The cases were ascertained in individuals with phenotypes including DD, ID, ASD or autistic features, epilepsy, abnormal EEG, hypotonia, dysmorphisms, microcephaly, and macrocephaly. Heterozygous *PPFIA3* variants were identified in nineteen individuals (1–19). One individual (20) was found to harbor compound heterozygous variants with concordant phenotypes. The variants from all affected individuals were identified through ES or Sanger sequencing.

Eleven of the individuals harbored *de novo* (1–2, 7–8, 10–15, and 17) missense variants. The *de novo* p.Arg429Trp variant was seen in individual 10 in a mosaic state (present in 26% of the ES reads, suggesting heterozygosity in ~52% of cells) from DNA analysis of fetal skin. Individuals 14 and 15 are monozygotic twins from family 13, and one individual (5) inherited a consensus splice variant from a similarly affected parent (6) (both from family 5). Individual 19 inherited a deletion of exons 22–30 from an affected parent, individual 20 inherited compound heterozygous variants from unaffected parents, and the inheritance pattern for six affected individuals is unknown (3, 4, 6, 9, 16, and 18) (Table 1, see supplemental information). The individuals with unknown inheritance pattern have either a missense variant (3, 4, and 9), a consensus splice variant (6), or a frameshift deletion (16 and 18).

To determine the potential pathogenicity of the *PPFIA3* variants, we examined the combined annotation-depletion (CADD) score where scores above 20 are considered to be deleterious.[44] The CADD scores for the *PPFIA3* variants ranged from 22.6 to 54, suggesting they are potentially deleterious (Table 2). Fourteen out of 17 variants were absent from the gnomAD (v.2.1.1).[37] The p.Arg784Trp variant had a frequency of 3.19×10^{-5} (1/31,386) in gnomAD v.2.1.1 and was identified as a *de novo* finding in individual 13 with mild ID and Landau-Kleffner epilepsy syndrome. The p.Pro793Thr variant had a frequency of 7.61×10^{-4} (215/282,366) in gnomAD v.2.1.1 and was identified as a maternally inherited variant *in trans* with a paternally inherited p.Lys759Arg variant in individual 20 with DD, ID, hypotonia, epilepsy, microcephaly, and autistic features. The p.Lys759Arg variant has a frequency of 4.77×10^{-5} (13/282,880) in gnomAD v.2.1.1. Differences in variant frequencies were documented in gnomAD v.4.0.0, encompassing variants reported in this study that were either submitted to ClinVar or identified from the UK Biobank (Tables S4 and S5).

Eighteen individuals in the cohort had DD and ID (1–6, 8–9, 11–20) (Tables S4 and S5, see supplemental information), while two individuals (7 and 10) could not be assessed for this feature due to premature mortality. Individual 7 had renal failure, severe anorectal malformation with complete anal atresia, absent bladder, dysmorphisms, and passed away at 5 months of age. Individual 10 had a prenatal diagnosis of abnormal gyration and ventriculomegaly, which led to elective pregnancy termination. Abnormal EEG (seen in 9/20; 1–3, 8, 9, 13, 17, 18, 20) and epilepsy (seen in 6/20; 1–3, 8, 13, 20) were found in a total of nine individuals (Table 1, see supplemental information). The affected individuals had multiple seizure semiologies including focal clonic seizures, atonic seizures, absence seizures, and focal tonic-clonic seizures with secondary generalization (Tables S4 and S5, see supplemental information).

Table 1. Genetic and neurologic findings in individuals with rare *PPFIA3* variants and neurodevelopmental disorders

Individual	1	2	3	4	5	6	7	8	9	10
Family	F1	F2	F3	F4	F5	F5	F6	F7	F8	F9
cDNA (GenBank: NM_003660.4)	c.115C>T	c.115C>T	c.118G>A	c.239A>C	c.240+1G>A	c.240+1G>A	c.943G>T	c.1243C>T	c.1243C>T	c.1285C>T
Protein (GenBank: NP_003651.1)	p.Arg39Cys	p.Arg39Cys	p.Glu40Lys	p.Gln80Pro	N/A	N/A	p.Ala315Ser	p.Arg415Trp	p.Arg415Trp	p.Arg429Trp
Human reference genome	GRCh37 (hg19)	GRCh37 (hg19)	GRCh37 (hg19)	GRCh37 (hg19)	GRCh37 (hg19)	GRCh37 (hg19)	GRCh37 (hg19)	GRCh37 (hg19)	GRCh37 (hg19)	GRCh37 (hg19)
Variant inheritance	*de novo*	*de novo*	not from mother; father unavailable for testing	unknown	inherited from affected mother (individual 6)	unknown	*de novo*	*de novo*	unknown	*de novo*
gnomAD (v.2.1.1)	not present	not present	not present	not present	not present	not present	not present	not present	not present	not present
Mosaicism	no	no	no	no	no	no	no	no	no	yes
Sex	male	male	female	female	female	female	female	female	female	female
Age at most recent assessment	16 years	13 years	22 years	1 year and 10 months	5 years	35 years	neonatal	8 years	10 years and 9 months	N/A
Racial and ethnic categories (NIH)	White	family declined to answer	White	White	White	White	Latino	mixed European and Asian	Asian	White
Status	alive	alive	alive	alive	alive	alive	deceased	alive	alive	elective pregnancy termination
Abnormal EEG	yes	yes	yes	N/A	N/A	N/A	N/A	yes	yes	N/A
Epilepsy	yes	yes	yes	no	no	no	N/A	yes	N/A	N/A
Autism or autistic features	no	no	no	suspected	no	N/A	N/A	autistic features	autistic features	N/A
Dysmorphisms	yes	yes	yes	yes	yes	yes	yes	yes	yes	N/A

Individual	11	12	13	14	15	16	17	18	19	20
Family	F10	F11	F12	F13	F13	F14	F15	F16	F17	F18
cDNA (GenBank: NM_003660.4)	c.1492C>T	c.1638G>T	c.2350C>T	c.2609T>A	c.2609T>A	c.2706dup	c.2717C>T	c.3307del	deletion exons 22–30	c.[2377C>A]; [c.2276A>G]
Protein (GenBank: NP_003651.1)	p.Arg498Trp	p.Trp546Cys	p.Arg784Trp	p.Ile870Asn	p.Ile870Asn	p.Ser903Leu fs*86	p.Ser906Leu	p.Glu1103Asnfs*8	N/A	p.[Pro793Thr]; p.[Lys759Arg]
Human reference genome	GRCh37 (hg19)	GRCh37 (hg19)	GRCh37 (hg19)	GRCh37 (hg19)	GRCh37 (hg19)	GRCh37 (hg19)	GRCh37 (hg19)	GRCh37 (hg19)	GRCh38 (hg38)	GRCh37 (hg19)
Variant inheritance	*de novo*	*de novo*	*de novo*	*de novo* (monozygotic twin of individual 15)	*de novo* monozygotic twin of individual 14)	unknown	*de novo*	unknown	inherited, affected mother	inherited from unaffected mother and father

(*Continued on next page*)

Table 1. ***Continued***

Individual	11	12	13	14	15	16	17	18	19	20
gnomAD (v.2.1.1)	not present	not present	frequency of 3.19×10^{-5} (1/31,386)	not present	not present	not present	not present	not present	N/A	p.Pro793Thr frequency of 7.61×10^{-4} (215/282,366); p.Lys759Arg frequency of 4.77×10^{-5} (13/282,880)
Mosaicism	no	no	no	no	no	N/A	no	no	N/A	none
Sex	male	male	female	female	female	male	female	female	male	male
Age at most recent assessment	6 years and 11 months	11 years	16 years	5 years	5 years	23 years	13 years and 11 months	9 years and 9 months	7 years and 8 months	9 years
Racial and ethnic categories (NIH)	Asian	White	White	White	White	White	White	White	White	White
Status	alive	alive	alive	alive	alive	alive	alive	alive	alive	alive
Abnormal EEG	N/A	no	yes	N/A	N/A	N/A	yes	yes	no	yes
Epilepsy	no	no	yes	no	no	N/A	no	no	no	yes
Autism or autistic features	yes, autistic features improved over last few years	yes	no	yes	no	autistic features	yes	no	N/A	autistic features
Dysmorphisms	Yes	no	no	no	no	N/A	yes	yes	yes	yes

Abbreviations: electroencephalogram (EEG), no information available (N/A).

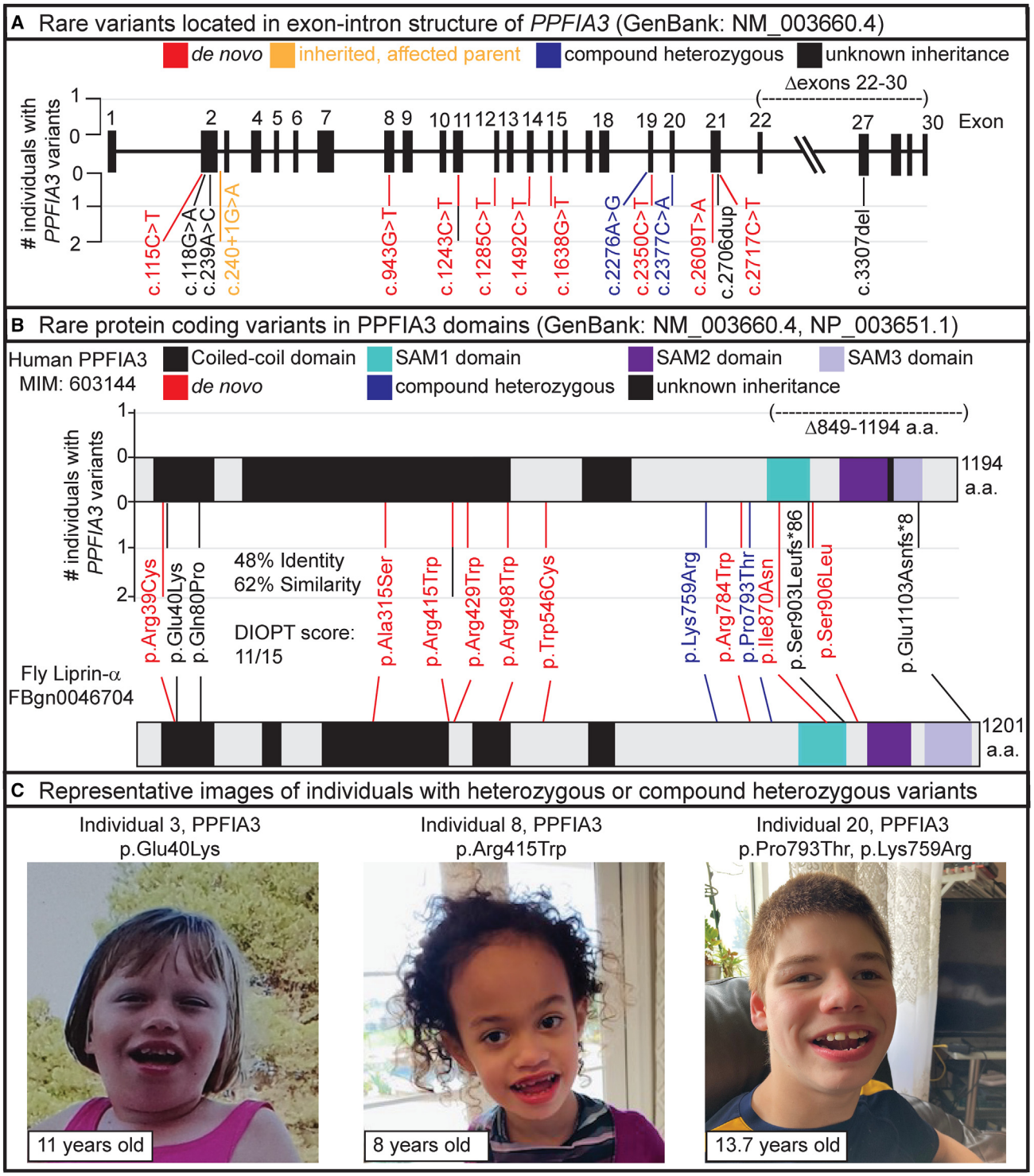

Figure 1. Variant location and images of individuals with PPFIA3 variants

(A) Location of *PPFIA3* variants in the genomic locus corresponding to the exon-intron structure. Number of individuals with the rare *PPFIA3* variant shown in the y axis.

(B) Location of *PPFIA3* variants in the corresponding protein domains. Number of individuals with the variant shown in the y axis. The fruit fly ortholog Liprin-α shows 48% identity and 62% similarity with the human PPFIA3. Sterile alpha motif, SAM.

(C) Images of individuals with heterozygous or compound heterozygous *PPFIA3* variants. The three individuals shown have dysmorphic features such as wide mouth, widely spaced teeth, prominent forehead, and hypotonic facies.

Six individuals had neuroanatomical changes detected by magnetic resonance imaging (MRI) (2, 3, 8, 10, 15, 20), which included flattening of the posterior globes at the level of optic nerve insertion, abnormal gyration with ventriculomegaly, and mild periventricular leukomalacia with mild white matter volume loss (Tables S4 and S5). Delayed

Table 2. *In silico* predictions for *PPFIA3* variants

Individuals	1 and 2	3	4	5 and 6	7	8 and 9	10	11
Human reference genome	GRCh37 (hg19)	GRCh37 (hg19)	GRCh37 (hg19)	GRCh37 (hg19)	GRCh37 (hg19)	GRCh37 (hg19)	GRCh37 (hg19)	GRCh37 (hg19)
PPFIA3 variant cDNA (GenBank: NM_003660.4)	c.115C>T	c.118G>A	c.239A>C	c.240+1G>A	c.943G>T	c.1243C>T	c.1285C>T	c.1492C>T
PPFIA3 variant protein (GenBank: NP_003651.1)	p.Arg39Cys	p.Glu40Lys	p.Gln80Pro	N/A	p.Ala315Ser	p.Arg415Trp	p.Arg429Trp	p.Arg498Trp
REVEL (v.1)	0.316	0.271	0.338	N/A	0.218	0.21	0.295	0.273
CADD (v.1.6)	31	30	26.8	34	24	33	29.2	25.9
GERP	4.19	4.19	4.34	4.34	4.29	2.12	2.95	1.41
M-CAP (v.1.4)	possibly pathogenic	possibly pathogenic	possibly pathogenic	N/A	possibly pathogenic	likely benign	possibly pathogenic	possibly pathogenic
PolyPhen2 HumDiv	probably damaging	probably damaging	benign	N/A	benign	probably damaging	probably damaging	probably damaging
PolyPhen2 HumVar	probably damaging	probably damaging	benign	N/A	benign	probably damaging	probably damaging	probably damaging
Phylop Vertebrate	0.945	9.447	9.02	N/A	9.4308	0.0498	2.25	2.58
SIFT	damaging	damaging	damaging	N/A	damaging	damaging	damaging	damaging

Individuals	12	13	14 and 15	16	17	18	19	20	20
Human reference genome	GRCh37 (hg19)	GRCh37 (hg19)	GRCh37 (hg19)	GRCh37 (hg19)	GRCh37 (hg19)	GRCh37 (hg19)	GRCh38 (hg38)	GRCh37 (hg19)	GRCh37 (hg19)
PPFIA3 variant cDNA (GenBank: NM_003660.4)	c.1638G>T	c.2350C>T	c.2609T>A	c.2706dup	c.2717C>T	c.3307del	deletion exons 22–30[a]	c.2377C>A	c.2276A>G
PPFIA3 variant protein (GenBank: NP_003651.1)	p.Trp546Cys	p.Arg784Trp	p.Ile870Asn	p.Ser903Leu fs*86	p.Ser906Leu	p.Glu1103Asnfs*8	N/A	p.Pro793Thr	p.Lys759Arg
REVEL (v.1)	0.186	0.158	0.41	N/A	0.207	N/A	N/A	0.092	0.183
CADD (v.1.6)	25.6	26.5	31	N/A	29.3	54	49	22.6	26.8
GERP	3.87	3.63	4.45	4.45	3.31	4.29	N/A	4.91	4.17
M-CAP (v.1.4)	possibly pathogenic	possibly pathogenic	possibly pathogenic	N/A	likely benign	N/A	N/A	possibly pathogenic	possibly pathogenic
PolyPhen2 HumDiv	probably damaging	probably damaging	probably damaging	N/A	tolerated	N/A	N/A	probably damaging	probably damaging
PolyPhen2 HumVar	probably damaging	benign	probably damaging	N/A	probably damaging	N/A	N/A	probably damaging	probably damaging
Phylop Vertebrate	4	1.609	7.855	N/A	5.756	N/A	N/A	3.7	9.17
SIFT	tolerated	damaging	damaging	N/A	damaging	N/A	N/A	damaging	damaging

Abbreviations: combined annotation-dependent depletion (CADD); genomic evolutionary rate profiling (GERP); Mendelian clinically applicable pathogenicity (M-CAP); polymorphism phenotyping v2 (PolyPhen2); sorting intolerant from tolerant (SIFT); not applicable (N/A)[a]no further information is available for the breakpoints for deletion in Individual 19.

speech development was present in 16 individuals (1–5, 8, 9, 11, 13–20) with absent speech in two individuals (8 and 20) (Tables S4–S6, see supplemental information). Hypotonia was present in eight individuals (1, 4, 8, 15, 17–20) (Tables S4 and S5, see supplemental information). Comorbid ASD diagnosis was reported in four individuals (11, 12, 14, 17) (Table 1, see supplemental information). Five of the individuals had autistic features, but no formal diagnosis of autism was made (4, 8, 9, 16, 20) (Table 1, see supplemental information). Gastrointestinal dysmotility characterized by constipation, difficulty feeding, and dysphagia was present in ten individuals (1, 3, 4, 7–9, 13–15, 20) (Tables S4 and S5, see supplemental information). Dysmorphic facial features were described in 13 individuals, which included prominent forehead, plagiocephaly, triangular face, clinodactyly, strabismus, wide mouth, widely spaced teeth, and bilateral epicanthal folds (1–5, 7–9, 11, 17–20) (Tables 1, S4 and S5; Figure 1C, see supplemental information). Macrocephaly or microcephaly were present in nine individuals (5–8, 14, 15, 17, 19, 20) (Tables S4 and S5, see supplemental information).

Conservation analysis and molecular modeling of *PPFIA3* variants

The predicted pathogenicity of *PPFIA3* variants was validated *in vivo* using *D. melanogaster* (fruit fly). The fly ortholog of *PPFIA3* is *Liprin-α*, and the fly protein shows an overall 48% identity and 62% similarity with the human protein (Figure 1B). Like the human PPFIA3, the fruit fly Liprin-α contains N-terminal coiled-coil domains and three C-terminal SAM domains (Figure 1B). Seven of the variants, p.Arg39Cys, p.Glu40Lys, p.Gln80Pro, p.Ala315Ser, p.Arg415Trp, p.Arg429Trp, and p.Arg498Trp, are located in the N-terminal coiled-coil domain (Figure 1B). The variants p.Ile870Asn and p.Ser903Leufs*86 are located in the SAM1 domain (Figure 1B). The variants p.Trp546Cys, p.Lys759Arg, p.Arg784Trp, p.Pro793Thr, and p.Ser906Leu are in the intrinsically disordered region of the protein; however, p.Ser906Leu is located near the SAM1 domain (Figure 1B). Conservation analysis of p.Arg39, p.Gln80, p.Ala315, p.Arg415, and p.Arg429 reveals these coiled-coil domain residues are well conserved in invertebrates and vertebrates. However, p.Glu40 is only conserved in mice and p.Arg498 is only conserved in mice and worms (Figure S1). The affected residues in the SAM1 domain, p.Ile870 and p.Ser903, and the residue near the SAM1 domain, p.Ser906, are also conserved across species. In the intrinsically disordered region, p.Trp546 is conserved in mice but not in fruit flies and worms; p.Lys759 is conserved in mice and fruit flies; p.Arg784 is conserved only in mice; and p.Pro793 is conserved only in mice (Figure S1). The affected variant in the SAM3 domain, p.Glu1103, is conserved in mice and fruit flies but not in worms (Figure S1).

Molecular modeling was completed for the missense variants using PyMol to determine whether the amino acid changes affect protein function *in silico* (Figures 2A and 2B). Regarding the coiled-coil variants, the variant p.Arg415Trp introduces a bulky side chain predicted to disrupt the interaction with p.Gln411 (Figure 2Ai). Similarly, the variant p.Arg429Trp introduces a bulky side chain that may disrupt the interaction with p.Asp424 (Figure 2Aii). The variant p.Arg784Trp introduces a bulky side chain predicted to disrupt the polar interaction with p.Asp785 (Figure 2Bi). The variant p.Ser906Leu is near the SAM1 domain and disrupts the interaction with the neighboring residue p.Ser908 (Figure 2Bii). Together, the molecular modeling suggests that these rare variants may hinder PPFIA3 function by disrupting the polar interactions with neighboring residues.

In vivo functional analysis of *PPFIA3* missense variants in fruit flies

To study the functional consequences of *PPFIA3* variants *in vivo*, we selected five of the missense variants to generate transgenic fruit flies using human cDNAs. We generated *UAS-PPFIA3*-WT-*HA*, *UAS-PPFIA3*-p.Arg39Cys-*HA*, *UAS-PPFIA3*-p.Ala315Ser-*HA*, *UAS-PPFIA3*-p.Arg415Trp-*HA*, *UAS-PPFIA3*-p.Trp546Cys-*HA*, and *UAS-PPFIA3*-p.Arg784Trp-*HA* fly alleles with C-terminal HA epitope tags (Table S7). The GAL4-UAS expression system was used to express *PPFIA3* WT and variant cDNAs under the spatiotemporal regulation of the transactivator protein GAL4 (Figure S2A). A pan-neuronal driver on the second chromosome, *elav-GAL4*, was used to express *PPFIA3* cDNAs in neurons, and a ubiquitous driver on the second chromosome, *Actin-GAL4*, was used to express *PPFIA3* cDNAs in the whole fly (Figure S2A). We found that *elav-GAL4* and *Actin-GAL4* produced the HA-tagged PPFIA3 WT and variants in third-instar larval brains (Figure S2B) and adult fly heads (Figure 2C). Interestingly, we observed elevated protein levels for PPFIA3 p.Arg39Cys compared to PPFIA3 WT and the other missense variants (Figures 2Ci, 2Cii, and S3). To confirm the cDNA copy-number insertions are consistent between the *PPFIA3* WT and variant fly lines, genomic DNA qPCR using SYBR Green was performed in *UAS-PPFIA3*-WT-*HA*, *UAS-PPFIA3*-p.Arg39Cys-*HA*, *UAS-PPFIA3*-p.Ala315Ser-*HA*, *UAS-PPFIA3*-p.Arg415Trp-*HA*, *UAS-PPFIA3*-p.Trp546Cys-*HA*, and *UAS-PPFIA3*-p.Arg784Trp-*HA*. Genomic DNA regions for *HA* epitope tag, *PPFIA3*, and *rps17* were amplified, and the expression levels of either *HA* or *PPFIA3* were quantified using *rps17* as the internal control (Figures S2Ci–S2Cii). We also performed semi-quantitative genomic DNA PCR using Taq polymerase, and the PCR product band intensity was quantified using *rps17* as the internal control (Figures S4 and S5). No significant difference in the relative expression of *HA* and *PPFIA3* was observed by both genomic DNA qPCR and PCR analyses, indicating the cDNA copy number is similar across all the *UAS-PPFIA3* WT and variant fly lines. Hence, the higher protein levels observed for p.Arg39Cys may be due to increased protein stability from the missense variant.

To determine whether expression of *PPFIA3* WT and missense variants are deleterious to developmental

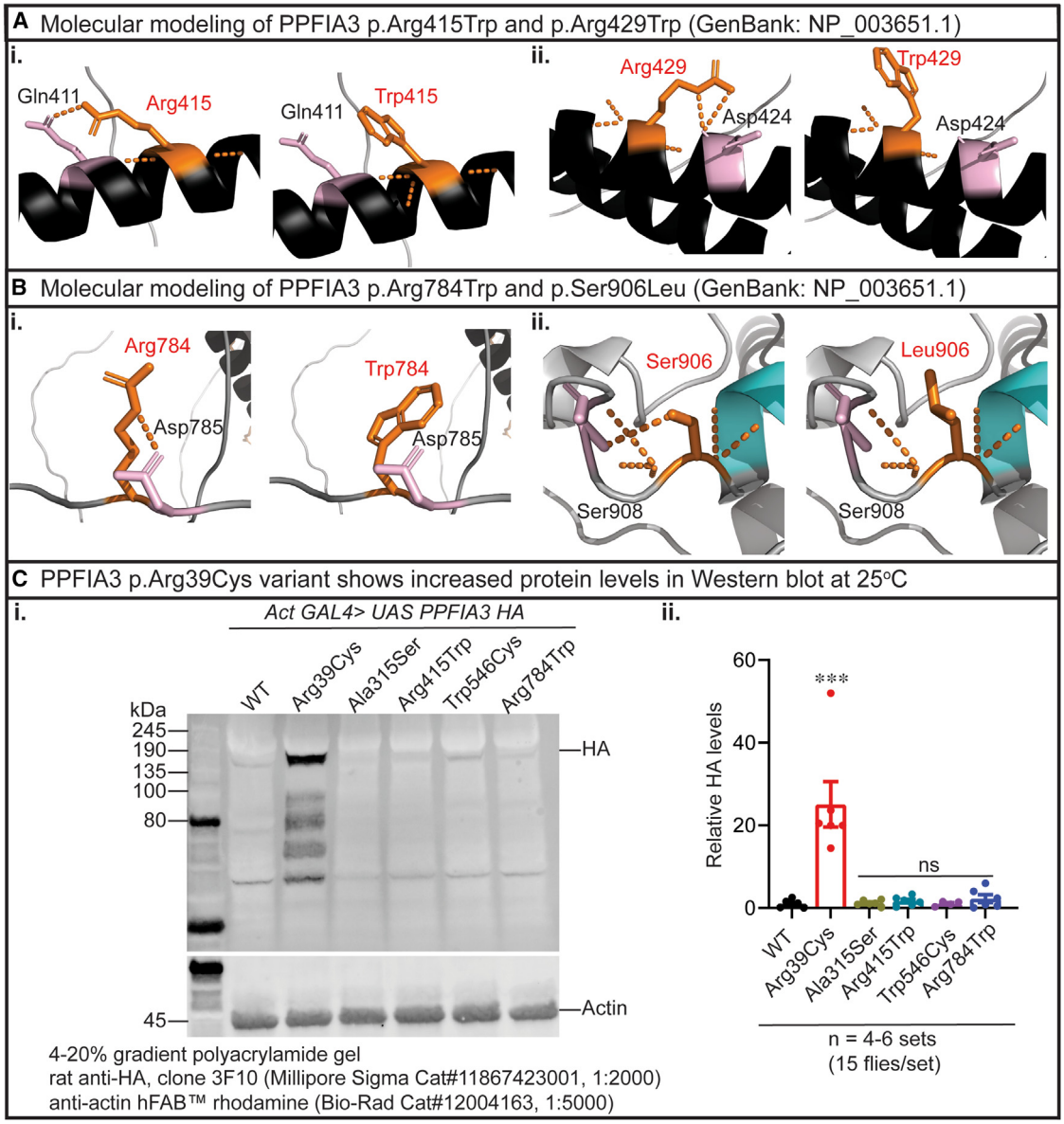

Figure 2. Molecular modeling of *PPFIA3* missense variants and protein levels associated with *PPFIA3* variants

(A and B) PPFIA3 missense variants are modeled in PyMol (version 2.5.2) with GenBank: NP_003651.1. Human PPFIA3 WT residues are modeled in gray with coiled coils displayed in black and affected residues highlighted in orange. Local polar contacts (orange dashed lines) and residue interactions (highlighted in pink) are displayed before and after mutagenesis for (Bi) p.Arg415Trp, (Bii) p.Arg429Trp, (Ci) p.Arg784Trp, and (Cii) p.Ser906Leu.

(C) (i) Western blot from PPFIA3 WT and variants show higher levels of HA in PPFIA3 p.Arg39Cys compared to WT.

(ii) Quantification of relative HA in 4–6 sets of biological replicates show higher level of HA in PPFIA3 p.Arg39Cys flies. Statistical analysis conducted with one-way ANOVA and Tukey's post-hoc analysis. Data shown as mean ± SEM. Significance shown as ***$p < 0.001$. Non-significance shown as ns.

processes, we ubiquitously expressed *PPFIA3* cDNAs using *Actin-GAL4* at 25°C and analyzed the fly development from pupal stage. *PPFIA3* cDNAs were expressed in the presence of endogenous fly *Liprin-α*. We found that PPFIA3 p.Arg39Cys causes pupal lethality and eclosion defects, whereas p.Ala315Ser and p.Arg415Trp cause only eclosion defect (Figures 3Ai and 3Aii). However, these phenotypes were not observed for the PPFIA3 p.Trp546Cys and p.Arg784Trp variants that are located in the intrinsically disordered region (Figures 3Ai–3Aii). In the eclosed adult flies, we observed a reduced penetrance of leg dysmorphology. The typical WT morphology is comprised of three pairs of legs with each leg containing three segments: femur, tibia, and tarsus (Figure 3Bi). We found morphological defects in these segments in either the first, second, third, or all leg pairs with expression of the *PPFIA3* missense variants (Figure 3Bi). Leg dysmorphology was observed in 80% of PPFIA3 p.Arg39Cys flies, 50% of PPFIA3 p.Ala315Ser flies, and 40% of PPFIA3 p.Arg415Trp flies (Figures 3Bi–3Bii). In PPFIA3 p.Arg784Trp flies, 10%

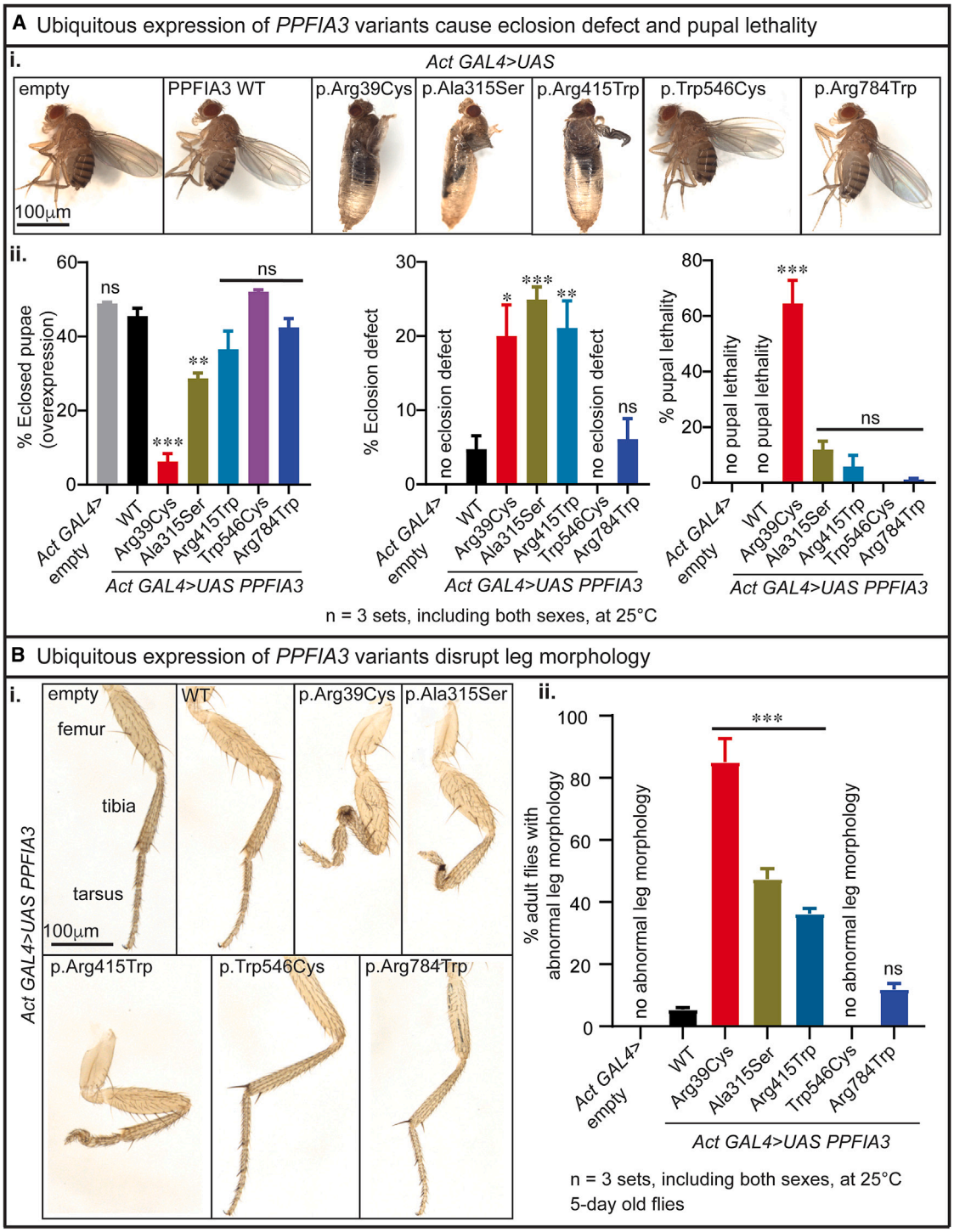

Figure 3. ***Actin-GAL4*-mediated ubiquitous expression of *PPFIA3* variants cause developmental and anatomical defects in fruit flies**

(A) Pupal lethality and eclosion defect associated with *Actin-GAL4*-mediated overexpression of *PPFIA3* variants.

(i) Images showing overexpression of PPFIA3 p.Arg39Cys cause pupal lethality and eclosion defect, and p.Ala315Ser and p.Arg415Trp cause eclosion defect compared to the PPFIA3 WT and *UAS*-empty control. Uneclosed flies from p.Arg39Cys, p.Ala315Ser, and p.Arg415Trp remain in the pupal case. PPFIA3 p.Trp546Cys and p.Arg784Trp overexpression does not cause a difference in pupal lethality and eclosion defect compared to PPFIA3 WT and *UAS*-empty control flies. Scale bar = 100 μm.

(ii) Bar graphs showing the percentage of eclosed pupae (overexpression), eclosion defect, and pupal lethal. Statistical analysis conducted with one-way ANOVA and Tukey's post-hoc analysis. Data shown as mean ± SEM with the sample size of total number of pupae in three sets. Significance shown as **$p < 0.01$ and ***$p < 0.001$. Non-significance shown as ns.

(B) Images of leg morphology associated with *Actin-GAL4*-mediated overexpression of *PPFIA3* variants.

(legend continued on next page)

had leg defects but the phenotype was not significant compared to that of PPFIA3 WT flies (Figures 3Bi–3Bii). In contrast, the leg dysmorphology phenotype was absent in the PPFIA3 p.Trp546Cys flies (Figures 3Bi–3Bii).

Next, to determine whether the neuronal expression of *PPFIA3* variants by *elav-GAL4* at 25°C impaired nervous system development and function, we conducted climbing behavior, bang-sensitivity behavior, and NMJ-morphology assays. First, we performed a climbing assay in 5-day-old flies to assess for motor defects. The standard behavior of the flies is to climb upward, and any increase in time to climb represents a potential defect in either motor coordination or negative geotaxis. Therefore, we used the climbing assay primarily as a screening tool to assess motor function. We found that *elav-GAL4>UAS-PPFIA3* WT flies had motor function like control flies that do not produce human PPFIA3 (*elav-GAL4>UAS*-empty) (Figure 4A). However, climbing behavior was impaired in PPFIA3 p.Arg39Cys-, p.Ala315Ser-, p.Arg415Trp-, and p.Arg784Trp-expressing 5-day-old flies (Figure 4A). Second, to determine whether the *PPFIA3* variants have electrophysiological abnormalities in the nervous system, we used bang sensitivity as a screening tool in the 5-day-old flies with 10-s vortexing. We found that *elav-GAL4>UAS-PPFIA3* WT flies were not bang sensitive and recovered similarly to the *elav-GAL4>UAS*-empty control. However, p.Arg39Cys, p.Ala315Ser, and p.Arg415Trp flies exhibited bang sensitivity with an increased recovery time (Figure 4B). When we examined the recovery time by sex, we found that p.Arg39Cys shows increased recovery time in males (Figure S6A), p.Ala315Ser shows increased recovery time both in males and females (Figure S6A), and p.Arg415Trp shows increased recovery time in females (Figure S6A). To determine whether there is an age-dependent effect, the climbing and bang assays were also performed in 15-day-old flies. We found that both p.Arg39Cys and p.Arg415Trp flies had climbing defects (Figure S6B). The bang-sensitivity assay for 15-day-old flies with 15-s vortexing showed recovery times similar to the bang-sensitivity assay in the 5-day-old flies (Figure S6B). Third, to explore the consequence of *PPFIA3* variants at the synapse, we examined the fruit fly third-instar larval NMJ morphology in muscle 6/7 of A3 (Figures 4Ci–4Cii). The fly NMJ is a glutamatergic synapse and a well-established model for excitatory glutamatergic synapse development and function.[45,46] We found a reduced number of boutons (presynaptic contacts) with *elav-GAL4*-mediated production of the PPFIA3 p.Arg39Cys and p.Arg415Trp variants (Figure 4Ciii), indicating that these variants perturb synapse formation. Total NMJ length associated with the *PPFIA3* variants were like the *PPFIA3* WT and *UAS*-empty controls (Figure 4Civ).

To determine the functional nature of the human *PPFIA3* variants in the absence of WT fly *Liprin-α*, we performed *in vivo* rescue experiments at 20°C–21°C with a previously established *Liprin-α* LOF allele,[32] *Liprin-α*^{F3ex15}, and a *Liprin-α* deficiency allele, *Df(2L)Exel7027/CyO* (Figure 5Ai). To express *PPFIA3* cDNAs in the background of *Liprin-α* LOF, we used the ubiquitously expressing *daughterless-GAL4* (*da-GAL4*). First, we observed that complete loss of *Liprin-α* function (*Liprin-α*^{F3ex15}/*Df(2L)Exel7027*) is embryonic lethal in control *da-GAL4>UAS*-empty flies, with a few escapers reaching larval stage (Figure 5Aii). We expressed the human *PPFIA3* WT or variant cDNAs in the background of *Liprin-α* LOF using a ubiquitously expressed *da-GAL4* at 20°C and assessed whether human PPFIA3 WT or variants rescued the embryonic lethality. We found a ∼25% larval rescue of embryonic lethality with PPFIA3 WT, indicating functional conservation in fruit flies (Figure 5Aii). PPFIA3 p.Arg39Cys and p.Arg415Trp resulted in significantly reduced larval rescue compared to WT (8% and 13%, respectively) (Figure 5Aii). However, the PPFIA3 p.Trp546Cys and p.Arg784Trp variants resulted in ∼17% rescue efficiency of the embryonic lethality, which was similar to the PPFIA3 WT rescue efficiency. Second, we assessed the survival of the rescued larvae to the adult stage (Figure 5Bi). We found that ∼35% of PPFIA3 WT larvae reached the adult stage; however, none of the PPFIA3 p.Arg39Cys larvae reached the adult stage (Figure 5Bii). In contrast, we found that 23% of PPFIA3 p.Arg415Trp larvae reached the adult stage, which is significantly reduced compared to PPFIA3 WT (Figure 5Bii). However, the frequency of PPFIA3 p.Trp546Cys and PPFIA3 p.Arg784Trp larvae reaching the adult stage was similar to PPFIA3 WT (33% and 30%, respectively) (Figure 5Bii). Third, we assessed the survival of these rescue adult flies in the 48-h post-eclosion. We found that 75% of PPFIA3 WT rescue flies were alive 48 h post-eclosion, indicating PPFIA3 WT in the *Liprin-α* LOF background is capable of restoring viability and survival. In contrast, only 35% of the PPFIA3 p.Arg415Trp and 30% of the PPFIA3 p.Arg784Trp rescue flies were alive 48 h post-eclosion (Figure 5Biii). However, PPFIA3 p.Trp546Cys rescue flies had a survival rate similar to PPFIA3 WT rescue flies (Figure 5Biii).

Finally, we analyzed the number of NMJ boutons and NMJ length with *da-GAL4*-mediated production of PPFIA3 WT and variants in the *Liprin-α* LOF background at 20°C (Figure S7A). Although the total number of boutons is significantly reduced compared to *da-GAL4>UAS*

(i) Empty control and PPFIA3 WT flies have typical legs with three segments. PPFIA3 p.Arg39Cys, p.Ala315Ser, and p.Arg415Trp result in pronounced leg segment developmental defects compared to PPFIA3 WT. Mild leg segmental developmental defects found with PPFIA3 p.Arg784Trp but not significant compared to PPFIA3 WT. No leg defects were found in PPFIA3 p.Trp546Cys flies. Scale bar = 100 μm. (ii) Bar graph showing the percentage of flies with abnormal leg morphology. Statistical analysis conducted with one-way ANOVA and Tukey's post-hoc analysis. Data shown as mean ± SEM with the sample size of total number of adult flies in three sets. Significance shown as ***$p < 0.001$. Non-significance shown as ns.

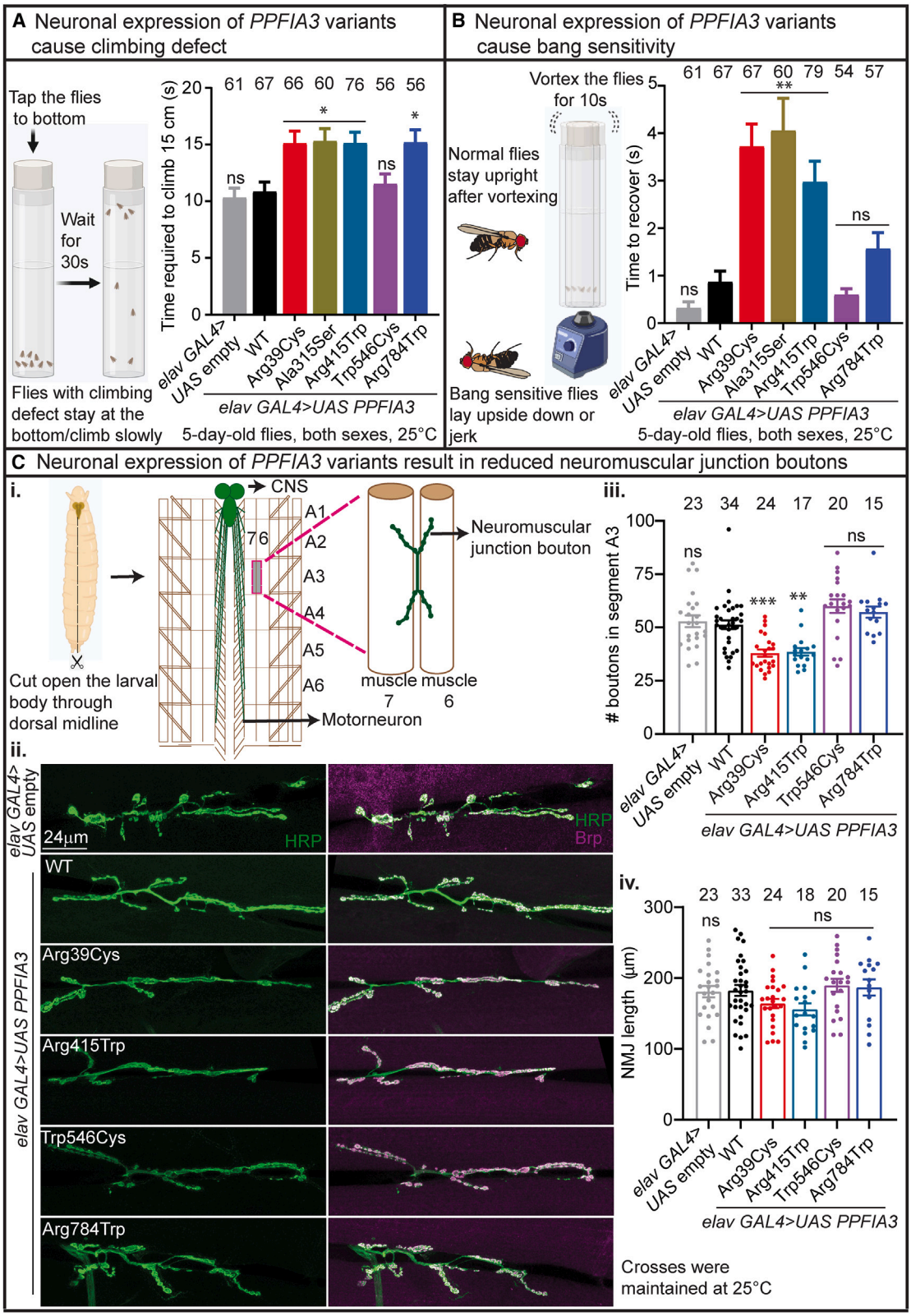

Figure 4. *elav-GAL4*-mediated neuronal overexpression of *PPFIA3* variants result in climbing defect, bang sensitivity, and neuromuscular junction (NMJ) bouton loss

(A) *elav-GAL4* mediated neuronal expression of PPFIA3 p.Arg39Cys, PPFIA3 p.Ala315Ser, PPFIA3 p.Arg415Trp, and PPFIA3 p.Arg784Trp result in impaired motor coordination on the climbing assay compared to PPFIA3 WT and empty control flies. Crosses were set and maintained at 25°C. Behavioral testing was conducted at 20°C–21°C with both sexes.

(legend continued on next page)

empty controls, there is no significant difference in the number of boutons between PPFIA3 WT and variants (Figure S7Bi). We quantified the total length of the NMJ and found no significant difference between genotypes (Figure S7Bii). Interestingly, we observed a significantly reduced ratio of bouton numbers per muscle 6/7 NMJ (segment A3) length in both PPFIA3 WT and variants compared to the *da-GAL4>UAS* empty control (Figure S7Bii). However, the bouton-to-NMJ-length ratio remained unchanged between PPFIA3 WT and variants (Figure S7Bii). This indicates that there is a significant loss of bouton density in the background of complete *Liprin-α* LOF compared to the *da-GAL4>UAS* empty control. However, neither PPFIA3 WT nor variants were able to rescue the loss of NMJ boutons in the *Liprin-α* LOF background (Figure S7Bi, iii). It is possible that due to the severity of the complete *Liprin-α* LOF, the PPFIA3 WT or variants expressing larvae examined for NMJ morphology represent a healthier subset of larvae capable of developing to the third-instar stage. Therefore, we may not be capturing PPFIA3 WT or variants expressing larvae with more severe NMJ phenotypes. This would limit our ability to identify a morphological difference between PPFIA3 WT and variants in the background of complete *Liprin-α* LOF. Together, the *in vivo* fly functional experiments demonstrate that rare *PPFIA3* variants p.Arg39Cys, p.Arg415Trp, and p.Arg784Trp result in loss of PPFIA3 function and are deleterious to multiple developmental processes. The clinical findings and fruit fly functional assays show that the *PPFIA3* variants have a variable spectrum of severity. The variants in the coiled-coil domains are associated with multiple neurodevelopment phenotypes in the affected individuals, and these variants cause severe phenotypes in the fruit flies as well (Table 3). These findings show that rare autosomal-dominant or autosomal-recessive *PPFIA3* variants in key functional domains may lead to a syndromic neurodevelopmental disorder.

Discussion

We describe 20 individuals from 18 families with 17 rare variants in *PPFIA3* who have neurodevelopmental phenotypes including DD, ID, hypotonia, ASD or autistic features, dysmorphisms, microcephaly or macrocephaly, abnormal EEG, and epilepsy (see supplemental information). The results of our clinical analysis, *in silico* molecular modeling, and *in vivo* functional studies in fruit flies show that rare *PPFIA3* variants lead to a syndromic neurodevelopmental disorder. PPFIA3 domain analysis and molecular modeling revealed that seven of the *PPFIA3* missense variants, p.Arg39Cys, p.Glu40Lys, p.Gln80Pro, p.Ala315Ser, p.Arg415Trp, p.Arg429Trp, and p.Arg498Trp, are located in the N-terminal coiled-coil domain. The coiled-coil domain is critical for PPFIA3's homodimerization and interaction with active zone proteins, such as RIM and ELKS, to regulate active zone organization and synaptic vesicle release.[13–16] Five PPFIA3 missense variants, p.Trp546Cys, p.Lys759Arg, p.Arg784Trp, p.Pro793Thr, and p.Ser906Leu, are located in the intrinsically disordered region of the protein. The p.Pro793Thr and p.Lys759Arg variants were inherited *in trans* from unaffected parents. One PPFIA3 missense variant, p.Ile870Asn, is located in the SAM1 domain. The SAM domains are known to bind to RNA, lipid membranes, and the adhesion molecule LAR-RPTP.[18,47,48] Finally, the PPFIA3 frameshift deletion variants (p.Ser903Leufs*86 and p.Glu1103Asnfs*8) and the exonic deletion variant (Δexons 22–30) may result in nonsense-mediated decay followed by reduced protein levels.

Phenotypic assessment of available clinical information revealed seven commonly reported neurodevelopmental features in the 20 individuals. These seven features include DD, ID, hypotonia, dysmorphisms, microcephaly or macrocephaly, ASD or autistic features, abnormal EEG, and epilepsy (Tables 1, S4, and S5, see supplemental information). We found that out of the nine individuals with missense variants in the coiled-coil domain (1 and 2, p.Arg39Cys; 3, p.Glu40Lys; 4, p.Gln80Pro; 7, p.Ala315Ser; 8 and 9, p.Arg415Trp; 10, p.Arg429Trp; and 11, p.Arg498Trp), two individuals had premature mortality (7 and 11). Individuals 1 and 2 have the same variant (p.Arg39Cys) and share similar clinical features such as abnormal EEG, epilepsy, DD, and ID. Individual 3 had DD, severe ID, hypertonia, dysmorphisms, and epilepsy.

(B) *elav-GAL4*-mediated neuronal expression of PPFIA3 p.Arg39Cys, PPFIA3 p.Ala315Ser, and PPFIA3 p.Arg415Trp have bang sensitivity with delayed recovery from vortexing compared to PPFIA3 WT and *UAS*-empty control flies. Crosses were set and maintained at 25°C. Behavioral test was conducted at 20°C–21°C with both sexes.
(C) *elav-GAL4*-mediated neuronal overexpression of *PPFIA3* variants result in NMJ bouton loss without a significant change in NMJ length.
(i) Model depicting the method for visualizing the NMJ in fruit fly third-instar larva.
(ii) Representative images of third-instar larval NMJs of each genotype including *elav GAL4>UAS* empty, *elav GAL4>PPFIA3* WT, p.Arg39Cys, p.Arg415Trp, p.Trp546Cys, and p.Arg784Trp are shown. Horseradish peroxidase (HRP) is a pan-neuronal marker (green) and Brp (Bruchpilot) is an active zone marker (magenta). Scale bar is 24 μm.
(iii) Quantification of total number of boutons in the muscle 6/7 (abdominal segment 3) NMJ show that PPFIA3 p.Arg39Cys and p.Arg415Trp result in bouton loss compared to PPFIA3 WT and empty control. In contrast, PPFIA3 p.Trp546Cys and p.Arg784Trp show no alteration in bouton numbers.
(iv) Quantification of total NMJ length in each genotype is shown, and there is no significant difference between PPFIA3 WT, variants, and *UAS*-empty control. Crosses were set and maintained at 25°C. Statistical analysis conducted with one-way ANOVA and Tukey's post-hoc analysis. Data shown as mean ± SEM with the sample size of total number of quantified NMJs shown above the bars. Significance shown as $^{**}p < 0.01$, $^{***}p < 0.001$. Non-significance shown as ns.

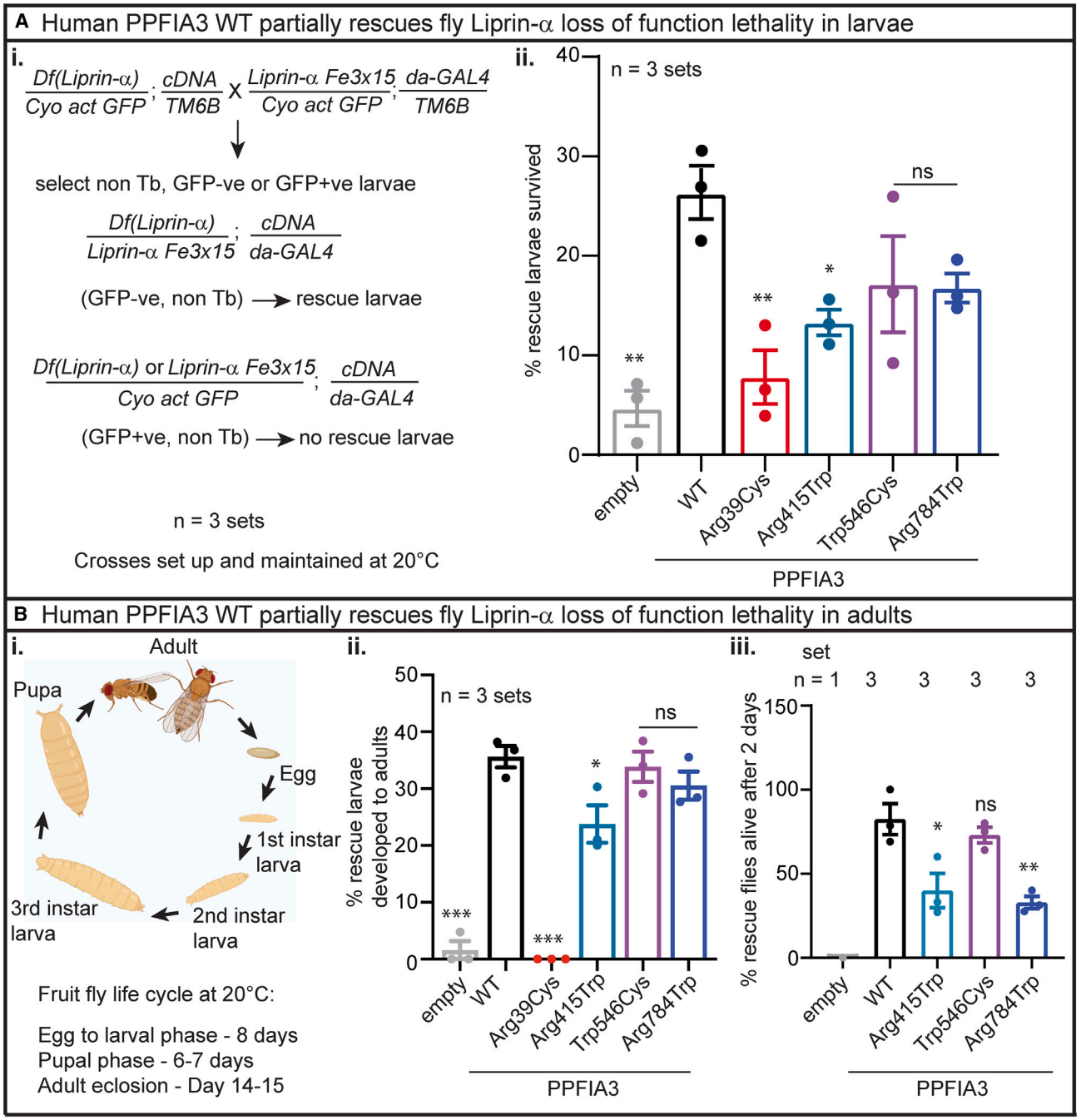

Figure 5. PPFIA3 WT partially rescues the fly Liprin-α LOF lethality

(A) Human PPFIA3 WT in the background of fly Liprin-α LOF results in a partial rescue of embryonic lethality.

(i) Crossing scheme to delete fly *Liprin-α* and express human *PPFIA3* WT and variants. The scheme describes the rescue larvae selection strategy. Crosses were set and maintained at 20°C.

(ii) Quantification of n = 3 sets per genotype showing % GFP-negative larvae (rescue larvae) that survive to the larval stage. PPFIA3 WT expression can partially rescue larval viability compared to empty control. PPFIA3 p.Arg39Cys and p.Arg415Trp show impaired ability to rescue larval viability.

(B) Human PPFIA3 WT expression partially rescues the lethality in adult stage.

(i) Representative illustration of the different stages of fruit fly development.

(ii) Quantification of 3 sets of rescued larvae per genotype that survive to the adult stage. PPFIA3 WT expression can partially rescue adult viability compared to empty control. PPFIA3 p.Arg39Cys and p.Arg415Trp show impaired ability to rescue adult viability.

(iii) Quantification of 1–3 sets of rescued larvae per genotype that survived after 48 h post-eclosion. For the empty control larvae, only one escaper rescue larvae survived to adult stage but died within 2 days post-eclosion. None of the PPFIA3 p.Arg39Cys rescue larvae survived to adult stage. Due to the lack of any PPFIA3 p.Arg39Cys rescue larvae surviving to the adult stage, this variant was not quantifiable

(legend continued on next page)

Individual 4 had autistic features, DD, ID, hypotonia, and dysmorphisms. Individuals 8 and 9 have the same variant (p.Arg415Trp), in which individual 8 had abnormal EEG, epilepsy, autistic features, DD, ID, hypotonia, dysmorphisms, and macrocephaly. Individual 9 had bilateral epileptiform discharges on EEG, autistic features, DD, and ID. Individual 11 had autism, DD, and ID. Our amino acid conservation analysis showed that affected residues in the PPFIA3 coiled-coil domain are highly conserved, except for the residues p.Glu40 and p.Arg498, across mice, fruit flies, and *C. elegans* (Figures S1A and S1B). These findings suggest the affected residues are critical for the protein's function across different species. Furthermore, molecular modeling of p.Arg415Trp and p.Arg429Trp variants suggested that the missense variants would hinder PPFIA3 function.

Three individuals have *de novo PPFIA3* missense variants (12, p.Trp546Cys; 13, p.Arg784Trp; and 17, p.Ser906Leu) in the intrinsically disordered region of the protein. The amino acid conservation analysis suggests that the affected residues are not well conserved across species except for p.Ser906 that is near the SAM1 domain. Individual 12 had autism, DD, and ID, whereas individual 13 had epilepsy, DD, and ID. Individual 17 (p.Ser906Leu) had abnormal EEG, autism, DD, ID, hypotonia, dysmorphisms, and micro/macrocephaly. Together, these findings suggest that variants in the intrinsically disordered regions are associated with variable disease severity, which may be due to the lack of association in this region with functional domains for PPFIA3. Two monozygotic twins had *PPFIA3* missense variants in the SAM1 domain (14 and 15, p.Ile870Asn). Individual 14 had autism, DD, ID, and microcephaly, and individual 15 had DD, ID, hypotonia, and microcephaly. Individual 18 has a *PPFIA3* frameshift variant in the SAM3 domain, p.Glu1103Asnfs*8, with abnormal EEG, DD, ID, hypotonia, and dysmorphisms. There were two related individuals (5 and 6) with a *PPFIA3* intronic splice variant (c.240+1G>A) and DD, ID, dysmorphisms, and microcephaly. Individual 5 inherited the *PPFIA3* variant from the affected parent, individual 6. The inheritance of the *PPFIA3* variant in individual 6 is unknown. One individual (20) was identified with compound heterozygous variants, p.Pro793Thr and p.Lys759Arg, which were inherited from asymptomatic parents. This individual has DD, ID, epilepsy, autistic features, hypotonia, dysmorphism, and microcephaly. As this is the only individual with biallelic variants in *PPFIA3* described to date in GeneMatcher,[38–40] the significance of these variants is uncertain until additional individuals with similar features and biallelic *PPFIA3* variants are identified. However, there are striking similarities in facial features and clinical phenotypes between individual 20 and other individuals in the cohort. Finally, we also identified a rare missense PPFIA3 p.Arg559Trp (c.1675C>T [GenBank: NM_003660.4]) variant of unknown inheritance in an individual with a discordant severe neurodegeneration phenotype and family history of consanguinity (data not shown). This variant is not present in gnomAD v.2.1.1 and has a CADD (v.1.6) score of 24.6, suggesting this variant could be potentially damaging. However, the severe neurodegeneration phenotype was not observed in the 20 individuals in our cohort. This suggests that PPFIA3 p.Arg559Trp is either a more severe deleterious variant or there are other genetic alterations, including alterations that may be related to the family history of consanguinity, contributing to this individual's clinical findings.

Our conservation analysis revealed that the PPFIA3 domains are well conserved in the fruit fly ortholog Liprin-α, which is primarily found in the fruit fly embryonic and larval nervous system. We utilized the evolutionary conservation to assess the impact of *PPFIA3* variants on development and behavior in the fruit fly. We found that ubiquitous expression of *PPFIA3* missense variants in the coiled-coil domain (p.Arg39Cys, p.Ala315Ser, and p.Arg415Trp) resulted in pupal lethality and/or eclosion defects. Interestingly, p.Arg39Cys caused severe pupal lethality, whereas p.Ala315Ser and p.Arg415Trp had milder effects on pupal lethality. All three tested variants in the coiled-coil domain showed abnormal leg morphology. Neuron-specific expression of PPFIA3 p.Arg39Cys and p.Arg415Trp variants showed bang sensitivity and climbing defects. Furthermore, as *Liprin-α* is known to regulate NMJ development in fruit flies, we examined the effect of human *PPFIA3* WT and variant cDNA expression in the larval NMJ. We found that PPFIA3 pArg39Cys and p.Arg415Trp caused a reduction in bouton number compared to PPFIA3 WT, which would potentially impair neurotransmission. Our fly overexpression findings reveal the *PPFIA3* missense variants in the coiled-coil domain cause lethality, suggesting these variants are dominant-negative alleles. Interestingly, ubiquitous or neuronal overexpression of the *PPFIA3* variants in the intrinsically disordered region (p.Arg784Trp and p.Trp546Cys) had either mild or no phenotypes in the fruit flies, which may be due to the variants not being conserved in the flies, causing mild protein dysfunction that is tolerated in the fly model, or these variants are benign and the phenotypes are due to other genetic etiologies. However, knowledge regarding the presence of Liprin-α outside the nervous system during Drosophila postembryonic development is limited.[32] Therefore, the genetic mechanism

for the adult survival phenotype. PPFIA3 p.Arg415Trp and PPFIA3 p.Arg784Trp show impaired ability to rescue adult viability compared to the PPFIA3 WT. Sample size is shown in Table S2. Statistical analysis with one-way ANOVA and Tukey's post-hoc analysis. Data shown as mean ± SEM with the sample size of flies scored shown in (Table S2). Significance shown as *$p < 0.05$, **$p < 0.01$, ***$p < 0.001$. Non-significance shown as ns.

Table 3. Comparison of clinical phenotypes and findings in fruit flies expressing *PPFIA3* missense variants

	PPFIA3 variants (GRCh37, hg19)	c.115C>T (p.Arg39Cys)		c.943G>T (p.Ala315Ser)	c.1243C>T (p.Arg415Trp)		c.1638G>T (p.Trp546Cys)	c.2350C>T (p.Arg784Trp)
	Individual	1	2	7	8	9	12	13
Key clinical phenotypes in individuals with *PPFIA3* variants	location	coiled-coil		coiled-coil	coiled-coil		disordered region	disordered region
	abnormal EEG	+	+	N/A	+	+	−	+
	epilepsy	+	−	N/A	+	−	−	+
	autism/autistic features	−	−	N/A	+	+	+	−
	DD/ID	+	+	N/A	+	+	+	+
	hypotonia	+	N/A	N/A	+	−	−	−
	dysmorphisms	+	+	+	+	N/A	−	−
	micro- or macrocephaly	−	−	+	+	N/A	−	−
	clinical features (# present/total reported)	5/7	3/6	2/2	7/7	3/5	2/7	3/7
Findings in fruit flies expressing *PPFIA3* variants	eclosion defect	+	+	+	−	−	−	+
	abnormal leg morphology	+	+	+	−	−	−	+
	climbing defect	+	+	+	−	+	−	+
	bang sensitivity	+	+	+	−	−	−	+
	NMJ defect	+	N/A	+	−	−	−	+
	liprin-α LOF rescue defect	+	N/A	+	−	+	−	+
	fly phenotypes (# present/total assays)	6/6	4/4	6/6	0/6	2/6	0/6	6/6
	variant severity according to the number of phenotypes in fly assays (0: no effect in fly assays; 1–2: mild; 3–4: moderate; 5–6: severe)	severe	at least moderate	severe	no effect	mild	no effect	severe

Abbreviations: electroencephalogram (EEG), delayed development (DD), intellectual disability (ID), no information available (n/a), loss of function (LOF), neuromuscular junction (NMJ).

underlying the *PPFIA3* variant-associated phenotypes in the fruit flies may be more complex.

To further determine whether the variants are LOF or gain of function (GOF) in nature and the functional conservation between human *PPFIA3* and fly *Liprin-α*, we performed an LOF lethality rescue assay using *Liprin-α* mutants and *PPFIA3* WT and variants. Our LOF rescue assay showed that human PPFIA3 WT partially rescued the Liprin-α LOF embryonic lethality and development to the adult stage, suggesting that human PPFIA3 WT function is partially conserved in fruit flies. Interestingly, the coiled-coil variants, PPFIA3 p.Arg39Cys and p.Arg415Trp, showed reduced rescue efficiency of the Liprin-α LOF embryonic lethality, indicating these variants are strong LOF variants. In contrast, the intrinsically disordered region variants, PPFIA3 p.Trp546Cys and p.Arg784Trp, showed a similar rescue efficiency of the embryonic lethality as compared to PPFIA3 WT. However, we found in the adult stage that PPFIA3 p.Arg784Trp significantly reduced the lifespan of rescue flies compared to PPFIA3 WT, suggesting that p.Arg784Trp is a hypomorphic LOF variant. These findings are consistent with the clinical findings in individuals 11 (p.Trp546Cys) and 12 (p.Arg784Trp). Both individuals had fewer clinical features reported. In contrast, individuals 1 and 2 (p.Arg39Cys) and individuals 8 and 9 (p.Arg415Trp) had more clinical features reported. Together, our overexpression and LOF rescue assays in fruit flies reveal that rare *PPFIA3* variants cause a neurodevelopmental disorder through an LOF mechanism and suggest that disease severity correlates with the degree of LOF.

Together, the clinical phenotypes and functional assays in fruit flies point toward a possible domain-specific disease-severity mechanism where the variants in the coiled-coil domains might lead to relatively more severe phenotypes in both affected individuals and fruit flies. Notably, ten individuals in the cohort have a family history of neurologic findings, which include ID, autism, NDD, dyslexia, muscular dystrophy, and psychiatric illnesses (Tables S4 and S5, see supplemental information). These familial findings raise the possibility that genetic background effects may also contribute to the severity and penetrance of *PPFIA3*-related phenotypes. However, the current number of participants and tested variants limits the prediction of genotype-phenotype correlations. Further studies in a larger sample size of affected individuals will be required to elucidate potential genotype-phenotype correlations.

Finally, to determine whether *PPFIA3* copy-number variants (CNVs) may potentially be contributory to neurodevelopmental phenotypes, we examined CNVs involving the *PPFIA3* locus in DECIPHER v.11.21, gnomAD structural variants (SVs) v.2.1, and ClinVar.[37,49,50] Across all three databases, seven individuals were reported with *PPFIA3* CNV deletions, but phenotypic information is limited to one individual reported with autistic behavior and mild microcephaly and one individual reported with a progressive familial heart block type IB (Figure S8A; Table S8). There are 82 individuals reported with chromosomal duplications in these databases (Figure S8A; Table S8). However, in gnomAD SV v.2.1, there were three individuals found to be homozygous and 38 individuals found to be heterozygous for a 42.9-kb duplication involving both the *PPFIA3* and *TRPM4* loci (Table S8), suggesting that *PPFIA3* duplication may be tolerated. Altogether, the phenotypes associated with the reported CNV deletions and duplications involving the *PPFIA3* locus include DD, ID, seizures, dysmorphisms, autistic behavior, microcephaly, and behavioral abnormalities (Figure S8; Table S8). Together, these findings suggest that *PPFIA3* deletions may contribute to the pathogenesis of neurodevelopmental disorders, but further studies will be needed to determine the significance of *PPFIA3* haploinsufficiency in human disease.

In summary, our study provides clinical and functional evidence that rare *PPFIA3* variants cause a syndromic neurodevelopmental disorder characterized by DD, ID, hypotonia, ASD or autistic features, dysmorphisms, and epilepsy. The reduced penetrance of features in affected family members suggests a complex relationship between *PPFIA3* germline variants and developmental features. Together, our *in vivo* functional modeling in fruit flies reveals that *PPFIA3* variants may contribute to disease pathogenesis through LOF mechanisms related to the location of the affected residues in the PPFIA3 functional domains. These findings and our clinical characterizations show that rare *PPFIA3* variants lead to a syndromic neurodevelopmental disorder. Future approaches to further elucidate the mechanistic underpinnings of *PPFIA3* variants in disease pathogenesis may include synaptic ultrastructural analysis with transmission electron microscopy, electrophysiology to analyze the synaptic recycling system, and genotype-to-phenotype correlations with fruit fly functional assays for the 17 identified *PPFIA3* variants. Longitudinal assessments in a larger sample size of affected individuals and mechanistic studies in model organisms will advance our understanding of disease pathogenesis, improve prognostication based on variant type and location, and identify potential therapeutic avenues.

Consortia

Members of the Undiagnosed Diseases Network (UDN) include Maria T. Acosta, Margaret Adam, David R. Adams, Raquel L. Alvarez, Justin Alvey, Laura Amendola, Ashley Andrews, Euan A. Ashley, Carlos A. Bacino, Guney Bademci, Ashok Balasubramanyam, Dustin Baldridge, Jim Bale, Michael Bamshad, Deborah Barbouth, Pinar Bayrak-Toydemir, Anita Beck, Alan H. Beggs, Edward Behrens, Gill Bejerano, Hugo J. Bellen, Jimmy Bennett, Beverly Berg-Rood, Jonathan A. Bernstein, Gerard T. Berry, Anna Bican, Stephanie Bivona, Elizabeth Blue, John Bohnsack, Devon Bonner, Lorenzo Botto, Brenna Boyd, Lauren C.

Briere, Gabrielle Brown, Elizabeth A. Burke, Lindsay C. Burrage, Manish J. Butte, Peter Byers, William E. Byrd, John Carey, Olveen Carrasquillo, Thomas Cassini, Ta Chen Peter Chang, Sirisak Chanprasert, Hsiao-Tuan Chao, Ivan Chinn, Gary D. Clark, Terra R. Coakley, Laurel A. Cobban, Joy D. Cogan, Matthew Coggins, F. Sessions Cole, Heather A. Colley, Heidi Cope, Rosario Corona, William J. Craigen, Andrew B. Crouse, Michael Cunningham, Precilla D'Souza, Hongzheng Dai, Surendra Dasari, Joie Davis, Jyoti G. Dayal, Esteban C. Dell'Angelica, Katrina Dipple, Daniel Doherty, Naghmeh Dorrani, Argenia L. Doss, Emilie D. Douine, Dawn Earl, David J. Eckstein, Lisa T. Emrick, Christine M. Eng, Marni Falk, Elizabeth L. Fieg, Paul G. Fisher, Brent L. Fogel, Irman Forghani, William A. Gahl, Ian Glass, Bernadette Gochuico, Page C. Goddard, Rena A. Godfrey, Katie Golden-Grant, Alana Grajewski, Don Hadley, Sihoun Hahn, Meghan C. Halley, Rizwan Hamid, Kelly Hassey, Nichole Hayes, Frances High, Anne Hing, Fuki M. Hisama, Ingrid A. Holm, Jason Hom, Martha Horike-Pyne, Alden Huang, Sarah Hutchison, Wendy Introne, Rosario Isasi, Kosuke Izumi, Fariha Jamal, Gail P. Jarvik, Jeffrey Jarvik, Suman Jayadev, Orpa Jean-Marie, Vaidehi Jobanputra, Lefkothea Karaviti, Shamika Ketkar, Dana Kiley, Gonench Kilich, Shilpa N. Kobren, Isaac S. Kohane, Jennefer N. Kohler, Susan Korrick, Mary Kozuira, Deborah Krakow, Donna M. Krasnewich, Elijah Kravets, Seema R. Lalani, Byron Lam, Christina Lam, Brendan C. Lanpher, Ian R. Lanza, Kimberly LeBlanc, Brendan H. Lee, Roy Levitt, Richard A. Lewis, Pengfei Liu, Xue Zhong Liu, Nicola Longo, Sandra K. Loo, Joseph Loscalzo, Richard L. Maas, Ellen F. Macnamara, Calum A. MacRae, Valerie V. Maduro, Audrey Stephannie Maghiro, Rachel Mahoney, May Christine V. Malicdan, Laura A. Mamounas, Teri A. Manolio, Rong Mao, Kenneth Maravilla, Ronit Marom, Gabor Marth, Beth A. Martin, Martin G. Martin, Julian A. Martínez-Agosto, Shruti Marwaha, Jacob McCauley, Allyn McConkie-Rosell, Alexa T. McCray, Elisabeth McGee, Heather Mefford, J. Lawrence Merritt, Matthew Might, Ghayda Mirzaa, Eva Morava, Paolo Moretti, John Mulvihill, Mariko Nakano-Okuno, Stanley F. Nelson, John H. Newman, Sarah K. Nicholas, Deborah Nickerson, Shirley Nieves-Rodriguez, Donna Novacic, Devin Oglesbee, James P. Orengo, Laura Pace, Stephen Pak, J. Carl Pallais, Christina G.S. Palmer, Jeanette C. Papp, Neil H. Parker, John A. Phillips III, Jennifer E. Posey, Lorraine Potocki, Barbara N. Pusey Swerdzewski, Aaron Quinlan, Deepak A. Rao, Anna Raper, Wendy Raskind, Genecee Renteria, Chloe M. Reuter, Lynette Rives, Amy K. Robertson, Lance H. Rodan, Jill A. Rosenfeld, Natalie Rosenwasser, Francis Rossignol, Maura Ruzhnikov, Ralph Sacco, Jacinda B. Sampson, Mario Saporta, Judy Schaechter, Timothy Schedl, Kelly Schoch, Daryl A. Scott, C. Ron Scott, Elaine Seto, Vandana Shashi, Jimann Shin, Edwin K. Silverman, Janet S. Sinsheimer, Kathy Sisco, Edward C. Smith, Kevin S. Smith, Lilianna Solnica-Krezel, Ben Solomon, Rebecca C. Spillmann, Joan M. Stoler, Kathleen Sullivan, Jennifer A. Sullivan, Angela Sun, Shirley Sutton, David A. Sweetser, Virginia Sybert, Holly K. Tabor, Queenie K.-G. Tan, Amelia L. M. Tan, Arjun Tarakad, Mustafa Tekin, Fred Telischi, Willa Thorson, Cynthia J. Tifft, Camilo Toro, Alyssa A. Tran, Rachel A. Ungar, Tiina K. Urv, Adeline Vanderver, Matt Velinder, Dave Viskochil, Tiphanie P. Vogel, Colleen E. Wahl, Melissa Walker, Stephanie Wallace, Nicole M. Walley, Jennifer Wambach, Jijun Wan, Lee-kai Wang, Michael F. Wangler, Patricia A. Ward, Daniel Wegner, Monika Weisz Hubshman, Mark Wener, Tara Wenger, Monte Westerfield, Matthew T. Wheeler, Jordan Whitlock, Lynne A. Wolfe, Kim Worley, Changrui Xiao, Shinya Yamamoto, John Yang, Zhe Zhang, and Stephan Zuchner.

Data and code availability

The de-identified data supporting the current study are available from the corresponding author on request. The submission and accession numbers for the variants reported to ClinVar are (1) individuals 1 and 2, Clin Var: SCV003804191.1; GenBank: NM_003660.4 (*PPFIA3*); c.115C>T (p.Arg39Cys); (2) individual 4, ClinVar: SCV003804194.1; c.239A>C (p.Gln80Pro); (3) individuals 8 and 9, ClinVar: SCV003804192.1; c.1243C>T (p.Arg 415Trp); (4) individual 10, ClinVar: SCV003801340; c.1285C>T (p.Arg429Trp); (5) individual 11, ClinVar: SCV003840201; c.1492C>T (p.Arg498Trp); (6) individual 12, ClinVar: SCV003804193.1; c.1638G>T (p.Trp546Cys); (7) individual 13, ClinVar: SCV003801341; c.2350C>T (p.Arg784Trp); (8) individuals 14 and 15, ClinVar: SCV004042691.1; c.2609T>A (p.Ile870Asn); (9) individual 17, ClinVar: SCV003035511; c.2717C>T (p.Ser906Leu); and (10) individual 18, ClinVar: SCV003035512; c.3307del (p.Glu1103Asnfs*8).

The following variants have been submitted to the ClinVar and the data are scheduled to be released publicly by April 29, 2024: (1) individual 3, ClinVar: SCV004041597; c.118G>A (p.Glu40Lys); (2) individuals 5 and 6, ClinVar: SCV004041598; c.240+1G>A; (3) individual 7, ClinVar: SCV004041599; c.943G>T; (p.Ala 315Ser); (4) individual 16, ClinVar: SCV004171207; c.27 06dup (p.Ser903Leufs*86); (5) individual 19, ClinVar: SCV004041600; deletion exons 22–30; (6) individual 20, ClinVar: SCV004041615; c.2377C>A; (p.Lys759Arg); and (7) individual 20, ClinVar: SCV004041614; c.2276A>G; (p.Pro793Thr).

Supplemental information

Supplemental information can be found online at https://doi.org/10.1016/j.ajhg.2023.12.004.

Acknowledgments

We thank the families and clinical staff at each location for participation in this study. In addition, we thank Mingshan Xue, Dongwon Lee, Kailin Mao, Wu (Charles) Chen, Brooke Horist, and Cole Deisseroth for critical feedback on the

manuscript. H.-T.C.'s research work is supported by the McNair Medical Institute at The Robert and Janice McNair Foundation, the Burroughs Wellcome Fund, Child Neurology Foundation and Society, the Gordan and Mary Cain Foundation, Annie and Bob Graham, The Elkins Foundation, and the Mark A. Wallace Endowment Award. M.S.P.'s research effort is supported in part by the National Ataxia Foundation and the Burroughs Wellcome Fund. J.M.P.'s research effort was supported in part by the Burroughs Wellcome Fund. V.C.L. and S.L.M. were supported in part by The Gordan and Mary Cain Foundation and Annie and Bob Graham. S.L.M. was also supported in part by the Mark A. Wallace Endowment Award. This work was also supported by Texas Children's Hospital, the Jan and Dan Duncan Neurological Research Institute, and the Eunice Kennedy Shriver National Institute of Child Health & Human Development of the National Institutes of Health under award number P50HD103555 for use of the Clinical Translational Core and Microscopy Core facilities. Research reported in this manuscript was supported by the NIH Common Fund, through the Office of Strategic Coordination/Office of the NIH Director under award number U01HG007709. The content is solely the responsibility of the authors and does not necessarily represent the official views of the National Institutes of Health.

Author contributions

M.S.P. and H.-T.C. contributed to the conception and design of the study, the acquisition and analysis of data, drafting the text, and preparing figures and tables. S.L.M., H.P., V.C.L., A.T., M.A.L., M.W.-H., R.A.L., M.R.B., N.B., L.M., S.P., J.T., J.L.M., S.R.C., L.L., T.P., D.Z., L.F., S.M., G.V., S.R.-H., G.L.C., C.A.B., B.H.L., H.Y.K., A.P., J.B., C.P., D.S.J.S., A.M., M.B.T., E.G.K., R.M., G.B.S., V.R., P.V., C.P., and M.O. contributed to the acquisition and analysis of data. J.M.P. and H.C. contributed to analysis of data and preparing figures. J.A.R., M.Z., M.W., H.E., K.C., E.M., M.J.G.S., R.P., P.P.M., A.S.A.C., J.-B.L.P., K.E., C.R., A-S.D.-P., S.S., I.E.S., and H.M. contributed to the acquisition and analysis of data, drafting the text, and preparing tables.

Declaration of interests

The Department of Molecular and Human Genetics at Baylor College of Medicine derives revenue from the clinical exome sequencing services offered at Baylor Genetics. J.L.M., M.J.G.S., and R.P. are employees of GeneDx, LLC.

Received: April 6, 2023
Accepted: December 4, 2023
Published: January 4, 2024

Web resources

CADD, https://cadd.gs.washington.edu/
ClinVAR, https://www.ncbi.nlm.nih.gov/clinvar/
CLUSTAL Omega, https://www.ebi.ac.uk/Tools/msa/clustalo/
Decipher, https://www.deciphergenomics.org/
DIOPT, https://fgr.hms.harvard.edu/diopt
GeneMatcher, https://genematcher.org/
gnomAD, https://gnomad.broadinstitute.org/
ImageJ, https://github.com/imagej/ImageJ
Imaris, https://imaris.oxinst.com/
MCAP, http://bejerano.stanford.edu/mcap/
OMIM, https://www.omim.org/
PyMOL, https://pymol.org/2/
SIFT, https://sift.bii.a-star.edu.sg/www/Extended_SIFT_chr_coords_submit.html
UCSC genome browser, https://genome.ucsc.edu/

References

1. Südhof, T.C. (2013). Neurotransmitter Release: The Last Millisecond in the Life of a Synaptic Vesicle. Neuron *80*, 675–690.
2. Südhof, T.C. (2004). The synaptic vesicle cycle. Annu. Rev. Neurosci. *27*, 509–547.
3. Zhai, R.G., and Bellen, H.J. (2004). The Architecture of the Active Zone in the Presynaptic Nerve Terminal. Physiology *19*, 262–270.
4. Xue, M., Giagtzoglou, N., and Bellen, H.J. (2011). Dueling Ca2+ Sensors in Neurotransmitter Release. Cell *147*, 491–493.
5. Südhof, T.C. (2012). The Presynaptic Active Zone. Neuron *75*, 11–25.
6. Hoischen, A., Krumm, N., and Eichler, E.E. (2014). Prioritization of neurodevelopmental disease genes by discovery of new mutations. Nat. Neurosci. *17*, 764–772.
7. Mencacci, N.E., Brockmann, M.M., Dai, J., Pajusalu, S., Atasu, B., Campos, J., Pino, G., Gonzalez-Latapi, P., Patzke, C., Schwake, M., et al. (2021). Biallelic variants in TSPOAP1, encoding the active-zone protein RIMBP1, cause autosomal recessive dystonia. J. Clin. Invest. *131*, e140625.
8. Lepeta, K., Lourenco, M.V., Schweitzer, B.C., Martino Adami, P.V., Banerjee, P., Catuara-Solarz, S., de La Fuente Revenga, M., Guillem, A.M., Haidar, M., Ijomone, O.M., et al. (2016). Synaptopathies: synaptic dysfunction in neurological disorders - A review from students to students. J. Neurochem. *138*, 785–805.
9. Taoufik, E., Kouroupi, G., Zygogianni, O., and Matsas, R. (2018). Synaptic dysfunction in neurodegenerative and neurodevelopmental diseases: an overview of induced pluripotent stem-cell-based disease models. Open Biol. *8*, 180138.
10. Chen, W., Cai, Z.-L., Chao, E.S., Chen, H., Longley, C.M., Hao, S., Chao, H.-T., Kim, J.H., Messier, J.E., Zoghbi, H.Y., et al. (2020). Stxbp1/Munc18-1 haploinsufficiency impairs inhibition and mediates key neurological features of STXBP1 encephalopathy. Elife *9*, e48705.
11. Serra-Pagès, C., Kedersha, N.L., Fazikas, L., Medley, Q., Debant, A., and Streuli, M. (1995). The LAR transmembrane protein tyrosine phosphatase and a coiled-coil LAR-interacting protein co-localize at focal adhesions. EMBO J. *14*, 2827–2838.
12. Serra-Pagès, C., Medley, Q.G., Tang, M., Hart, A., and Streuli, M. (1998). Liprins, a Family of LAR Transmembrane Protein-tyrosine Phosphatase-interacting Proteins. J. Biol. Chem. *273*, 15611–15620.
13. Taru, H., and Jin, Y. (2011). The Liprin Homology Domain Is Essential for the Homomeric Interaction of SYD-2/Liprin-α Protein in Presynaptic Assembly. J. Neurosci. *31*, 16261–16268.
14. Schoch, S., Castillo, P.E., Jo, T., Mukherjee, K., Geppert, M., Wang, Y., Schmitz, F., Malenka, R.C., and Südhof, T.C. (2002). RIM1α forms a protein scaffold for regulating neurotransmitter release at the active zone. Nature *415*, 321–326.
15. Ko, J., Na, M., Kim, S., Lee, J.-R., and Kim, E. (2003). Interaction of the ERC Family of RIM-binding Proteins with the

Liprin-α Family of Multidomain Proteins. J. Biol. Chem. *278*, 42377–42385.
16. Dai, Y., Taru, H., Deken, S.L., Grill, B., Ackley, B., Nonet, M.L., and Jin, Y. (2006). SYD-2 Liprin-α organizes presynaptic active zone formation through ELKS. Nat. Neurosci. *9*, 1479–1487.
17. Kim, C.A., and Bowie, J.U. (2003). SAM domains: uniform structure, diversity of function. Trends Biochem. Sci. *28*, 625–628.
18. Pulido, R., Serra-Pagès, C., Tang, M., and Streuli, M. (1995). The LAR/PTP delta/PTP sigma subfamily of transmembrane protein-tyrosine-phosphatases: multiple human LAR, PTP delta, and PTP sigma isoforms are expressed in a tissue-specific manner and associate with the LAR-interacting protein LIP.1. Proc. Natl. Acad. Sci. USA *92*, 11686–11690.
19. Van Der Lee, R., Buljan, M., Lang, B., Weatheritt, R.J., Daughdrill, G.W., Dunker, A.K., Fuxreiter, M., Gough, J., Gsponer, J., Jones, D.T., et al. (2014). Classification of Intrinsically Disordered Regions and Proteins. Chem. Rev. *114*, 6589–6631.
20. Babu, M.M. (2016). The contribution of intrinsically disordered regions to protein function, cellular complexity, and human disease. Biochem. Soc. Trans. *44*, 1185–1200.
21. Liu, Y.C., Couzens, A.L., Deshwar, A.R., B McBroom-Cerajewski, L.D., Zhang, X., Puviindran, V., Scott, I.C., Gingras, A.C., Hui, C.C., and Angers, S. (2014). The PPFIA1-PP2A protein complex promotes trafficking of Kif7 to the ciliary tip and Hedgehog signaling. Sci. Signal. *7*. ra117-13.
22. van der Vaart, B., van Riel, W.E., Doodhi, H., Kevenaar, J.T., Katrukha, E.A., Gumy, L., Bouchet, B.P., Grigoriev, I., Spangler, S.A., Yu, K.L., et al. (2013). CFEOM1-Associated Kinesin KIF21A Is a Cortical Microtubule Growth Inhibitor. Dev. Cell *27*, 145–160.
23. Shin, H., Wyszynski, M., Huh, K.-H., Valtschanoff, J.G., Lee, J.-R., Ko, J., Streuli, M., Weinberg, R.J., Sheng, M., and Kim, E. (2003). Association of the Kinesin Motor KIF1A with the Multimodular Protein Liprin-α. J. Biol. Chem. *278*, 11393–11401.
24. Spangler, S.A., Jaarsma, D., De Graaff, E., Wulf, P.S., Akhmanova, A., and Hoogenraad, C.C. (2011). Differential expression of liprin-α family proteins in the brain suggests functional diversification. J. Comp. Neurol. *519*, 3040–3060.
25. Zürner, M., and Schoch, S. (2009). The mouse and human Liprin-α family of scaffolding proteins: Genomic organization, expression profiling and regulation by alternative splicing. Genomics *93*, 243–253.
26. Zürner, M., Mittelstaedt, T., tom Dieck, S., Becker, A., and Schoch, S. (2011). Analyses of the spatiotemporal expression and subcellular localization of liprin-α proteins. J. Comp. Neurol. *519*, 3019–3039.
27. Wong, M.Y., Liu, C., Wang, S.S.H., Roquas, A.C.F., Fowler, S.C., and Kaeser, P.S. (2018). Liprin-α3 controls vesicle docking and exocytosis at the active zone of hippocampal synapses. Proc. Natl. Acad. Sci. USA *115*, 2234–2239.
28. Kang, H.J., Kawasawa, Y.I., Cheng, F., Zhu, Y., Xu, X., Li, M., Sousa, A.M.M., Pletikos, M., Meyer, K.A., Sedmak, G., et al. (2011). Spatio-temporal transcriptome of the human brain. Nature *478*, 483–489.
29. Zhen, M., and Jin, Y. (1999). The liprin protein SYD-2 regulates the differentiation of presynaptic termini in C. elegans. Nature *401*, 371–375.
30. Kittelmann, M., Hegermann, J., Goncharov, A., Taru, H., Ellisman, M.H., Richmond, J.E., Jin, Y., and Eimer, S. (2013). Liprin-α/SYD-2 determines the size of dense projections in presynaptic active zones in C. elegans. J. Cell Biol. *203*, 849–863.
31. Patel, M.R., and Shen, K. (2009). RSY-1 Is a Local Inhibitor of Presynaptic Assembly in *C. elegans*. Science *323*, 1500–1503.
32. Kaufmann, N., DeProto, J., Ranjan, R., Wan, H., and Van Vactor, D. (2002). Drosophila Liprin-α and the Receptor Phosphatase Dlar Control Synapse Morphogenesis. Neuron *34*, 27–38.
33. Astigarraga, S., Hofmeyer, K., Farajian, R., and Treisman, J.E. (2010). Three *Drosophila* Liprins Interact to Control Synapse Formation. J. Neurosci. *30*, 15358–15368.
34. Hofmeyer, K., Maurel-Zaffran, C., Sink, H., and Treisman, J.E. (2006). Liprin-α has LAR-independent functions in R7 photoreceptor axon targeting. Proc. Natl. Acad. Sci. USA *103*, 11595–11600.
35. Amberger, J., Bocchini, C.A., Scott, A.F., and Hamosh, A. (2009). McKusick's Online Mendelian Inheritance in Man (OMIM). Nucleic Acids Res. *37*, D793–D796.
36. Samocha, K.E., Robinson, E.B., Sanders, S.J., Stevens, C., Sabo, A., McGrath, L.M., Kosmicki, J.A., Rehnström, K., Mallick, S., Kirby, A., et al. (2014). A framework for the interpretation of de novo mutation in human disease. Nat. Genet. *46*, 944–950.
37. Karczewski, K.J., Francioli, L.C., Tiao, G., Cummings, B.B., Alföldi, J., Wang, Q., Collins, R.L., Laricchia, K.M., Ganna, A., Birnbaum, D.P., et al. (2020). The mutational constraint spectrum quantified from variation in 141,456 humans. Nature *581*, 434–443.
38. Arachchi, H., Wojcik, M.H., Weisburd, B., Jacobsen, J.O.B., Valkanas, E., Baxter, S., Byrne, A.B., O'Donnell-Luria, A.H., Haendel, M., Smedley, D., et al. (2018). *matchbox* : An open-source tool for patient matching via the Matchmaker Exchange. Hum. Mutat. *39*, 1827–1834.
39. Sobreira, N., Schiettecatte, F., Valle, D., and Hamosh, A. (2015). GeneMatcher: A Matching Tool for Connecting Investigators with an Interest in the Same Gene. Hum. Mutat. *36*, 928–930.
40. Philippakis, A.A., Azzariti, D.R., Beltran, S., Brookes, A.J., Brownstein, C.A., Brudno, M., Brunner, H.G., Buske, O.J., Carey, K., Doll, C., et al. (2015). The Matchmaker Exchange: A Platform for Rare Disease Gene Discovery. Hum. Mutat. *36*, 915–921.
41. Chao, H.-T., Davids, M., Burke, E., Pappas, J.G., Rosenfeld, J.A., McCarty, A.J., Davis, T., Wolfe, L., Toro, C., Tifft, C., et al. (2017). A Syndromic Neurodevelopmental Disorder Caused by De Novo Variants in EBF3. Am. J. Hum. Genet. *100*, 128–137.
42. Bischof, J., Sheils, E.M., Björklund, M., and Basler, K. (2014). Generation of a transgenic ORFeome library in Drosophila. Nat. Protoc. *9*, 1607–1620.
43. Gahl, W.A., Mulvihill, J.J., Toro, C., Markello, T.C., Wise, A.L., Ramoni, R.B., Adams, D.R., Tifft, C.J.; and UDN (2016). The NIH Undiagnosed Diseases Program and Network: Applications to modern medicine. Mol. Genet. Metabol. *117*, 393–400.
44. Kircher, M., Witten, D.M., Jain, P., O'Roak, B.J., Cooper, G.M., and Shendure, J. (2014). A general framework for estimating the relative pathogenicity of human genetic variants. Nat. Genet. *46*, 310–315.
45. Menon, K.P., Carrillo, R.A., and Zinn, K. (2013). Development and plasticity of the *Drosophila* larval neuromuscular

junction: Development and plasticity of the neuromuscular junction. WIREs Dev Biol *2*, 647–670.
46. Collins, C.A., and DiAntonio, A. (2007). Synaptic development: insights from Drosophila. Curr. Opin. Neurobiol. *17*, 35–42.
47. Green, J.B., Gardner, C.D., Wharton, R.P., and Aggarwal, A.K. (2003). RNA Recognition via the SAM Domain of Smaug. Mol. Cell *11*, 1537–1548.
48. Barrera, F.N., Poveda, J.A., González-Ros, J.M., and Neira, J.L. (2003). Binding of the C-terminal Sterile α Motif (SAM) Domain of Human p73 to Lipid Membranes. J. Biol. Chem. *278*, 46878–46885.
49. MacDonald, J.R., Ziman, R., Yuen, R.K.C., Feuk, L., and Scherer, S.W. (2014). The Database of Genomic Variants: a curated collection of structural variation in the human genome. Nucleic Acids Res. *42*, D986–D992.
50. Landrum, M.J., Lee, J.M., Benson, M., Brown, G.R., Chao, C., Chitipiralla, S., Gu, B., Hart, J., Hoffman, D., Jang, W., et al. (2018). ClinVar: improving access to variant interpretations and supporting evidence. Nucleic Acids Res. *46*, D1062–D1067.